Toward an integrative geological and geophysical view of Cascadia subduction zone earthquakes

Authors:
Maureen A.L. Walton[1] & Lydia M. Staisch[2], Tina Dura[3], Jessie K. Pearl[4], Brian Sherrod[4], Joan Gomberg[4], Simon Engelhart[5], Anne Tréhu[6], Janet Watt[1], Jon Perkins[2], Robert C. Witter[7], Noel Bartlow[8], Chris Goldfinger[6], Harvey Kelsey[9], Ann E. Morey[6], Valerie J. Sahakian[10], Harold Tobin[11], Kelin Wang[12], Ray Wells[2], Erin Wirth[4]

[1]US Geological Survey, Pacific Coastal and Marine Science Center
[2]US Geological Survey, Geology Minerals Energy and Geophysics Science Center
[3]Virginia Tech, Department of Geosciences, Blacksburg, VA
[4]US Geological Survey, Earthquake Science Center
[5]University of Durham, Department of Geography
[6]Oregon State University, College of Earth Ocean and Atmospheric Sciences
[7]US Geological Survey, Alaska Science Center
[8]University of Kansas, Department of Geology
[9]Humboldt State University, Department of Geology
[10]University of Oregon, Department of Earth Sciences
[11]University of Washington, Department of Earth and Space Sciences
[12]Geological Survey of Canada, Pacific Geoscience Centre

Keywords
Subduction zone, Pacific Northwest, earthquake, recurrence, megathrust

Summary Phrases

1. Despite outstanding geologic records of past megathrust events, large uncertainty of the magnitude and frequency of CSZ earthquakes remains
2. Here we outline current knowledge and promising future directions to address outstanding questions on CSZ rupture characteristics and recurrence
3. Integration of diverse datasets with attention to the geologic processes that create different records has potential to lead to major progress

Abstract

The Cascadia subduction zone (CSZ) is an exceptional geologic environment for recording evidence of land level changes, tsunamis, and ground motion that reveals at least 19 great megathrust earthquakes over the past 10 kyr. Such earthquakes are among the most impactful natural hazards on Earth, transcend national boundaries, and can have global impact. Reducing the societal impacts of future events in the U.S. Pacific Northwest and coastal British Columbia, Canada, requires improved scientific understanding of megathrust earthquake rupture, recurrence, and corresponding hazards. Despite substantial knowledge gained from decades of research, large uncertainties remain about the characteristics and frequencies of past CSZ earthquakes. In this review, we summarize geological, geophysical, and instrumental evidence relevant to understanding megathrust earthquakes along the CSZ and associated uncertainties. We discuss how the evidence constrains various models of great megathrust earthquake recurrence in Cascadia and identify potential paths forward for the earthquake science community.

1. Introduction

Subduction zones, where tectonic plates converge along plate boundary megathrust faults, produce some of the most devastating natural disasters globally: great (M>8.0) megathrust

earthquakes and their corresponding hazardous phenomena (Fig. 1). The 2004 M 9.2 Sumatra earthquake and tsunami killed 250,000 people in 15 countries, producing an international disaster. Even well-prepared countries can suffer catastrophic damage and loss of life, as in the 2011 M9.0 Tōhoku earthquake and tsunami in Japan (McGuire et al., 2017). These two catastrophes took the world by surprise and showed a need for better understanding of the seismic cycle and rupture variability in subduction zones. The Cascadia subduction zone (CSZ) of western North America (Fig 1) presents a unique opportunity to address major outstanding questions in subduction zone science (Gomberg et al., 2017). With better understanding of these powerful and complicated tectonic systems, we may improve future hazard preparation and maintain the safety and economic viability of affected populations.

Classic elastic theory (Reid, 1910) describes the subduction zone seismic cycle as a two-stage model in which the crust and uppermost-mantle deform elastically in response to far-field tectonic forces: 1) an interseismic period when strain accumulates (Fig. 2A), and 2) a coseismic period when an earthquake suddenly relieves the accumulated strain (Figure 2B). For a shallow-dipping subduction megathrust, gradual subsidence near the fault and uplift farther away characterizes interseismic upper plate deformation (Fig. 2A) and is followed by abrupt coseismic reversal of the deformation pattern (Fig. 2B). Global observations, however, reveal that the process of strain accumulation and release on faults is complex and that the *recurrence interval* for earthquakes can vary along a fault and through space and time (Sieh et al., 2008; Goldfinger et al., 2012; Kulkarni et al., 2013; Nocquet et al., 2017; Bilek & Lay, 2018). This presents challenges when trying to calculate future earthquake probabilities in order to prepare for and mitigate impacts from inevitable future events.

The Cascadia subduction zone (CSZ) extends for more than 1300 km from Cape Mendocino in northern California to Vancouver Island in southwestern British Columbia (McCrory et al., 2012) and has been accumulating strain for 320 years since the last great earthquake in 1700 CE (Atwater et al., 2005; McCaffrey et al., 2013). The next CSZ earthquake could be another ~M9 that ruptures the entire margin like the 1700 CE event, but also might be a series of smaller events occurring in quick succession (Fig. 2C). While recent earthquakes help to inform forecasts of potential earthquakes in other subduction zones (e.g., Alaska in 1946, 1957, 1964, 1965; Chile in 1960 & 2010; Sumatra in 2004 & 2007; Japan in 2011), geologic records underpin our understanding of earthquake rupture parameters and CSZ earthquake hazard assessments (Hemphill-Haley, 1995; Atwater et al., 2005; Kelsey et al., 2002; Witter et al., 2003; Nelson et al., 2008; Goldfinger et al., 2012; Frankel et al., 2015). Fortunately, Cascadia coastal and submarine environments preserve different aspects of past earthquake processes over millennial time scales and feature some of the best prehistoric earthquake catalogs in the world (Hutchinson, 1992; Long & Shennan, 1998; Goldfinger et al., 2012; Engelhart et al., 2015; Dura et al., 2016a).

The spatial and temporal robustness of geologic records in Cascadia provide a strong foundation to address outstanding questions on subduction zone science and earthquake recurrence-governing principles that remain elusive globally. However, questions about the timing and extent of past ruptures remain in Cascadia due to age-dating uncertainties resulting in non-unique interpretations of geologic records, unknown relative contributions of coseismic and postseismic motions, and unresolved structural and rheological controls on rupture extent. Furthermore, different rupture characteristics impact tsunami inundation, the extent of seismically triggered landslides, and the effects of geologic architecture on seismic wave amplification (Fig. 1; Geist, 2002; 2005; Frankel, 2013; Frankel et al., 2018; Wirth et al., 2018; Roten et al., 2019; Wirth & Frankel, 2019). In this review, we summarize the substantial knowledge gained over decades of subduction zone research in Cascadia, discuss subduction zone processes that create geologic archives of past earthquakes, and identify associated uncertainties and natural variability. We highlight remaining knowledge gaps in CSZ earthquake studies through a synthesis of available data and models and suggest pathways towards accurate

interpretation of the earthquake deformation cycle model that incorporates both geological and geophysical datasets.

2. Cascadia subduction zone earthquake evidence over the millennia: Geologic observations

The CSZ preserves the most spatially and temporally complete geologic records of past great megathrust earthquakes in the world (Atwater & Hemphill-Haley, 1997; Kelsey et al., 2002; 2005; Witter et al., 2003; Nelson et al., 2006; Goldfinger et al., 2012; 2017). Widespread low-energy, ecologically sensitive tidal wetlands and estuaries and isolated coastal lakes are excellent recorders of decimeter-scale interseismic and coseismic deformation and tsunami inundation (Figs. 1 and 2D; Witter et al., 2003; Engelhart et al., 2015; Dura et al., 2016a). Additionally, nearshore marine environments receive ample sediment supply for the generation and preservation of seismically triggered turbidites (Fig. 1; Goldfinger et al., 2012). In this section, we summarize existing geologic evidence that constrains the timing and rupture characteristics of past Cascadia megathrust events.

2.1. Onshore stratigraphic evidence of the earthquake deformation cycle

The stratigraphy beneath Cascadia's tidal wetlands reflects the strain accumulation and release of the earthquake deformation cycle (Fig. 2D). Bank sections and sediment cores preserve repeated sequences of organic-rich tidal wetland soils formed in the interseismic period, sharply overlain by tidal mud deposited following decimeter-scale coseismic subsidence (Fig. 3A & 3B; Darienzo et al., 1994; Atwater & Hemphill-Haley, 1997; Clague et al., 2000; Kelsey et al., 2002; Witter et al., 2003; Nelson et al., 2008). At some tidal wetland sites, sand and silt layers signaling high-energy tsunami inundation of the coast are evident at the soil-mud contact (Figs. 2D & 3B). In coastal lakes, landward thinning sand beds signal marine incursions from past tsunamis (Kelsey et al., 2005). Radiocarbon ages from pre- and post-earthquake and/or tsunami sediment bracket the timing of coseismic subsidence and/or tsunami inundation. Typical age uncertainty is on the order of a few hundred years; however, dendrochronological analysis of trees killed by rapid coseismic subsidence and marine inundation, particularly for events in the past 2000 years where sufficient wood has been preserved, has the potential to yield more precise ages (Fig. 2D; Atwater & Yamaguchi, 1991; Jacoby et al., 1995; 1997; Yamaguchi et al., 1997).

The completeness of onshore geologic archives of coseismic subsidence and/or tsunami inundation depends on the creation and preservation thresholds at a site, termed *evidence thresholds* (Nelson et al., 2006). In order to exceed the creation threshold at a site, the evidence of coseismic subsidence and/or tsunami inundation must be distinct from similar evidence produced by local non-seismic processes (Nelson et al., 2006). In order to exceed the preservation threshold at a site, the balance among erosional and depositional processes must favor the preservation of coseismic subsidence and/or tsunami inundation evidence. Holocene relative sea level (RSL) history and evidence thresholds at each site along the CSZ control the length and completeness of onshore geologic archives of coseismic subsidence and tsunami inundation (Engelhart et al., 2015; Dura et al., 2016a). The longest geologic archives of coseismic subsidence and tsunami inundation are in central and southern Cascadia, where gradual RSL rise since ~5-7 ka produces the accommodation space in tidal wetlands necessary for preservation (Atwater & Hemphill-Haley, 1997; Witter et al., 2003). In northern Cascadia (e.g., Vancouver Island), gradual RSL fall since ~6 ka limits the preservation of coseismic subsidence evidence to the last ~1-2 ka, and typically only the last ~500 years (Fig. 4; Dura et al., 2016a). Evidence of tsunami inundation in northern Cascadia extends to ~3.5 ka (Goff et al., 2020).

In order to distinguish stratigraphic contacts created by megathrust ruptures from other non-seismic processes (e.g., climate driven sea-level change, changes in estuary hydrography),

researchers consider several criteria: (1) the suddenness of the change in environment across the contacts; (2) the lateral extent of sharp stratigraphic contacts; (3) significant environmental change evident in microfossil assemblages across sharp contacts; (4) the continuity of stratigraphic evidence within a site and across multiple sites; and (5) the coincidence of tsunami deposits with sudden stratigraphic change (Darienzo et al., 1994; Nelson et al., 1996; Shennan et al., 1996, 2016). Satisfying criteria 1-4 implies that an earthquake produces the decimeters of subsidence necessary to exceed the evidence threshold (Nelson et al., 2006). The additional presence of an overlying tsunami deposit (criteria 5) strongly supports an offshore rupture, rather than localized wetland depositional processes.

The best-preserved and most widely documented megathrust earthquake in the onshore geologic record at the CSZ occurred in 1700 CE (Supplemental text; Nelson et al., 1995; Satake et al., 2003; Atwater et al., 2005; Goldfinger et al., 2012). Coastal wetlands spanning >1000 km of the CSZ preserve distinct soil-mud contacts, and anomalous accompanying silt or sand beds at the contacts signal sudden coseismic submergence and tsunami inundation of coastal environments (Figs. 1 & 2D; Atwater et al., 2005 & references therein). The 1700 CE tsunami propagated across the Pacific, causing inundation and damage along the coast of Japan (Satake et al., 2003; Atwater et al., 2005). Modeling of the arrival-time of tsunami waves documented in Japan, and dendrochronological dating of coastal trees simultaneously killed by coseismic subsidence in Washington, Oregon, and California, precisely constrain the age of the earthquake to January 26, 1700 CE (Atwater et al., 2005 & references therein). Tsunami modeling, along with the uniquely precise date and concurrence of evidence for this event, supports the inference that it was a full-margin, M8.7 - 9.2 rupture (Yamaguchi et al., 1997; Satake et al., 2003; Atwater et al., 2005; Nelson et al., 2020).

Stratigraphic- and microfossil-based estimates of coseismic subsidence in 1700 CE aid in assessing the rupture characteristics of the event, such as slip distribution. Early stratigraphic- and microfossil-based estimates of coseismic subsidence in 1700 CE often have uncertainties in excess of a meter (Hemphill-Haley, 1995; Dura et al., 2016b), and therefore highly simplified uniform-slip rupture models were permissible by earlier datasets (Wang et al., 2003; Leonard et al., 2004, 2010). More recent statistically based transfer function analyses use empirical relationships derived from modern foraminifera samples to estimate past marsh elevations from fossil foraminifera assemblages and have reduced subsidence uncertainty to 0.3-0.5 m at some sites (Hawkes et al., 2011; Kemp et al., 2018), though uncertainties due to contamination from possible short-term postseismic deformation remain (Horton et al., 2017). The more precise microfossil-based subsidence estimates resolve slip variability along the CSZ in 1700 CE and result in more realistic heterogeneous rupture models (Wang et al., 2013; Wirth & Frankel, 2019).

Gaining a deeper understanding of recurrence and slip behavior of past events along the CSZ requires geologic records that span multiple earthquake cycles (Leonard et al., 2004, 2010; Wirth & Frankel, 2019). Geologic studies in southern Washington and northernmost Oregon tidal wetlands (Shennan et al., 1996; Atwater & Hemphill-Haley, 1997; Nelson et al., 2006) document up to ten widely correlative buried soils representing coseismic subsidence over the last ~5000 years, with recurrence intervals between earthquakes ranging from a few decades to one millennium (average recurrence 500-540 years). In central and southern Oregon and northern California (Kelsey et al., 2002; Witter et al., 2003; Milker et al., 2016; Padgett et al., in review), tidal wetlands and coastal lakes preserve up to 12 earthquakes and/or tsunamis over the same ~5000 year time period (average recurrence ~390 years; Kelsey et al., 2002, 2005; Witter et al., 2003, 2012a). Geologic records reveal rupture patterns that suggest northern Cascadia commonly breaks in long ruptures, while southernmost Cascadia experiences more frequent ruptures of variable length (Nelson et al., 2006). Geologic records also show variable amounts of subsidence during successive earthquakes at some sites (Milker et al., 2016), and persistent low (Nelson et al., in review) or high (Kelsey et al., 2002) amounts of deformation at

other sites. Along-strike structural barriers at the CSZ (see section 3.2) potentially control the along-strike variability in rupture length and coseismic deformation over multiple earthquake cycles documented in onshore geologic datasets.

Tsunami deposits can provide clues about the time, location, and extent of the megathrust rupture source that complements other onshore paleoseismic evidence (Peters et al., 2007; Peterson et al., 2011). Earthquake-induced tsunamis occur when coseismic slip causes significant seafloor deformation and are sensitive to the depth and extent of rupture (Fig. 1D; Priest et al., 2014; Melgar et al., 2016). CSZ tsunami deposits generally consist of anomalous sandy to silty sediments extending kilometers inland from the shoreline, may contain marine microfossils, and often accompany coastal subsidence records (Fig. 4; Kelsey et al., 2002; 2005; Witter et al., 2003). Other tsunamigenic sources, such as crustal earthquakes and large submarine landslides, tend to produce localized tsunamis, whereas megathrust-generated tsunamis affect a broad region (Goldfinger et al., 2000; Garrison-Laney et al., 2017). At the CSZ, researchers use the inland extent, thickness, and grain size of tsunami deposits preserved along the CSZ to ground truth tsunami inundation simulations (Witter et al., 2013), estimate offshore slip during past tsunamigenic earthquakes (Witter et al., 2012a), and resolve the hydrodynamics of tsunami inundation (Witter et al., 2012b).

2.2. Marine turbidite records

Marine sediment cores in Cascadia record disturbance layers and evidence for turbidity currents, termed *turbidites*, generated from offshore coseismic ground shaking (Fig. 1B; Adams, 1990; Goldfinger et al., 2012). Turbidites can be found in abyssal channels, proximal canyons, fan systems, aprons, and slope basins, and typically consist of a sharp basal contact, a fine sandy-silty basal layer, and an upward-fining sequence of silt, mud, and clay (Fig. 3C). In southern Cascadia, subdued *mud turbidites* lack a sandy component in some locales (Goldfinger et al., 2012, 2013a).

Turbidites result from the shaking produced by megathrust and crustal earthquakes, as well as non-earthquake related processes such as storms (Goldfinger et al., 2012; Gavey et al., 2017, Howarth et al., 2018; Mountjoy et al., 2018); thus, distinguishing between multiple sources of event beds requires sedimentological arguments or physical criteria, often site-specific. One physiographic test is to look for consistent Holocene stratigraphy among site types that lack connections to each other or to terrestrial sources. The *confluence test* is another physiographic criterion used along the Cascadia margin where multiple channel systems and turbidity current pathways lead away from the filled trench. The confluence argument suggests that if the turbidity currents travel synchronously down the tributary channels and coalesce into a single channel to travel as one large turbidity current, then a margin-wide event, such as a great earthquake, likely triggered the density flows (Adams, 1990; Goldfinger et al., 2012). If multiple events trigger turbidity currents, then the tributary channels and the main channel should contain different numbers of turbidite deposits.

Most of the canyon systems of Cascadia are Pleistocene features, making Cascadia an ideal site for Holocene paleoseismology. There remains some debate about the Pleistocene to modern sediment routing in offshore channels and the infallibility of the confluence test (Atwater & Griggs, 2012; Atwater et al., 2014; Hill et al., 2020). While Holocene sediment supply is variable along the CSZ margin and can take a series of complex pathways that could obfuscate estimates of recurrence from the turbidite record (Atwater et al., 2014), Goldfinger et al. (2017) argue that consistent event-bed records among many site types and locales show that the earthquake signal commonly overprints local variability (see also Rong et al., 2014).

Multiple tributaries to the Cascadia Channel contain 19 Holocene sandy turbidites, 13 of which post-date the ~7630 yr old Mazama ash (Fig. 4; Adams, 1990; Goldfinger et al., 2012). Downstream, the count remains 13 post-Mazma events in most cores, suggesting synchronous deposition. Heavy mineral suites and hydrodynamic modeling support the independence of the

tributaries (Goldfinger et al., 2017) and the Adams (1990) confluence test. Juan de Fuca Channel, Hydrate Ridge slope basin, Rogue Apron, and Astoria Fan each contain 19 sandy turbidites (Fig. 4). These sandy turbidites share a common chronology estimated from ^{14}C ages and depositional age models, and log correlation methods assist in correlating them along-strike (Enkin et al., 2013; Hamilton et al., 2015; Goldfinger et al., 2012, 2017). The 1700 CE earthquake is the youngest turbidite in nearly all marine cores (Fig. 4). Compilation of turbidite events and onshore subsidence and tsunami records suggests a recurrence interval of 500 - 530 years for margin-wide (~M9) megathrust earthquakes (Goldfinger et al., 2012). In southern Cascadia at Hydrate Ridge, Rogue Apron, and sites extending to Eel Canyon, a series of 12 - 22 fine-grained turbidites intercalated between hemipelagic sediments and sandy turbidites have been interpreted as more frequent and limited southern CSZ rupture (Goldfinger et al., 2012).

Turbidite age estimates broadly overlap age ranges for onshore CSZ earthquake evidence, especially for the sandy turbidites representing the largest most widespread events (Witter et al., 2012a); however, some turbidites interpreted as earthquake-triggered events (e.g., T2) do not have corresponding onshore subsidence or tsunami evidence (Fig. 4). Differences in evidence thresholds can account for at least some discrepancies between onshore and offshore records (Nelson el al, 2006; Goldfinger et al., 2016). Onshore, subsidence thresholds may be as large as M_W 8.4 (Nelson et al., 2006), while the turbidite record includes events at least as low as M_W 7.1 (Goldfinger et al., 2019). For example, mud turbidites above the 1700 CE turbidite layer near Cape Mendocino likely correlate with the 1906 San Andreas and 1992 Petrolia earthquakes, suggesting that crustal M>7 earthquakes triggered these turbidity flows (Goldfinger et al., 2019). Thus, the turbidite record in southernmost Cascadia appears to include shorter CSZ ruptures as well as crustal earthquakes. The discrepancies in the datasets may alternatively suggest that not all margin-wide turbidites are seismically triggered, or that certain rupture characteristics optimize turbidite generation but do not generate onshore deformation and tsunamis.

2.3. Lacustrine turbidites and disturbance deposits

Lakes from a variety of settings are uniquely sensitive to shaking from different types of seismic sources and often provide long, continuous sediment records ideally suited for paleoseismic investigation (Vandekerkhove et al., 2020; van Daele et al., 2019; Praet et al., 2017; Moernaut et al., 2007); recent work indicates increasing utilization of lacustrine records in Cascadia earthquake science (Morey et al., 2013; Goldfinger et al., 2017; Leithold et al., 2018). Turbidites in Oregon and northern California lakes are of a similar timing and frequency (Morey et al., 2013) as the record of offshore seismogenic turbidites (Goldfinger et al., 2012).

Several studies suggest that lake sediments record locally generated ground shaking magnitude and source. Sedimentary records from Lake Washington, near Seattle, contain two event layers that coincide with known earthquakes, including the 1700 CE megathrust earthquake and an ~1100 yr old Seattle fault zone rupture; the other six events found in these records are from older earthquakes in the region and have recurrence intervals between 400 and 500 years, which may therefore indicate they were generated by megathrust rupture (Karlin et al., 2004). On the Olympic Peninsula, Lake Quinault sedimentary records contain three event layers in the last three thousand years (Leithold et al., 2018), suggesting either that only some CSZ earthquakes cause local ground shaking sufficient to create lacustrine disturbance events or that not all lakes are equally good earthquake recorders. Also on the Olympic Peninsula, Lake Crescent contains a sedimentary record with four major disturbance events that correlate to rupture along a nearby crustal fault, whereas thinner lake turbidite layers may be from megathrust, upper plate, and intraplate earthquakes that caused lesser local ground shaking (Leithold et al., 2019). On Vancouver Island, Effingham and Saanich inlets are deep anoxic inlets that effectively mimic lacustrine environments. Of the two records, the Saanich Inlet, well inland, shows evidence for nearly twice as many events (Blais-Stevens et al., 2011), whereas the Effingham inlet seems to record mainly plate boundary events. In addition, the Saanich Inlet

record may suggest that some CSZ megathrust earthquakes rupture only the northern portion of the megathrust (Blais-Stevens et al., 2011). The difference in these records highlights the sensitivity of local response to seismic source type and shaking characteristics.

2.4. Other onland proxies of strong ground shaking

Liquefaction from seismic shaking manifests as sedimentary intrusions (sills and dikes), vented sand deposits (Fig. 2D), soft sediment deformation, and lateral spreading. Previous surveys identify rare surficial liquefaction features in Cascadia (Obermeier, 1995; Takada & Atwater, 2004). Most evidence for seismically induced liquefaction in Cascadia comes from sedimentary outcrops along rivers and estuaries, such as swampy islands along the lower Columbia River and cut banks of the Chehalis River in southwestern Washington (Obermeier et al., 1993; Atwater, 1994; Obermeier, 1995; Obermeier & Dickenson, 2000; Takada & Atwater, 2004). Atwater (1994) describes outcrops on the banks on these islands with hundreds of centimeter-scale sand bodies intruding, and in some cases, venting onto the surface of a buried soil dated to the 1700 CE megathrust earthquake. Slices of subsurface deposits from the lower Columbia River show evidence of liquefaction from at least four great earthquakes in the past 2000 years (Takada and Atwater, 2004).

Subduction zone earthquakes sometimes radiate strong shaking and trigger landslides over broad areas (Figs. 1F & 3D), as seen in the 1960 Chilean, 1964 Alaska, and the 2011 Tohoku earthquakes (Hansen, 1965; Veblen & Ashton, 1978; Wartman et al., 2013). Researchers have yet to definitively connect any of Cascadia's abundant landslides to a megathrust rupture despite thorough surveys (Perkins et al., 2018; Hill et al., 2020, Struble et al., 2020; LaHusen et al., in press). The paucity of megathrust-triggered deep-seated landslides along the Cascadia margin may suggest that onshore ground shaking from past great earthquakes was not sufficiently strong. However, recent work suggests landslides from crustal earthquakes or major rainfall events overprints prior potential megathrust-generated landslides (Struble et al., 2020; LaHusen et al., in press).

Candidate megathrust-generated landslides include rock slides near Newport, OR, where modern observations of landslide reactivation rates suggest that it began moving around 1700 CE and continues to move today (Schulz et al., 2012). On the Olympic Peninsula, a terrace formed from a breached rockslide-dammed lake containing buried trees in growth position (Leithold et al., 2018) and a landslide-buried Makah fishing village (Kirk, 2015) may correlate to the 1700 CE event. Confirming seismic triggers for these sites requires robust age control.

3. Contemporary deformation: Constraints from instrumental and geophysical datasets

Determining whether geological boundaries are present and their impact on rupture propagation and megathrust behavior is a major challenge that requires integrating paleoseismic and contemporary geophysical data and comparing the CSZ to other subduction zones. In this section, we review evidence of interplate coupling and contemporary indications of seismic activity in the forearc and discuss what we can infer about earthquake behavior from seismic and geodetic observations. We use several terms to describe portions of the subduction zone exhibiting common slip behavior, and noting that some studies use these terms differently, we define them here as follows. The *seismogenic zone* is the part of the plate boundary where dynamic friction is less than the static friction and exhibits *stick-slip behavior*. This behavior is a prerequisite for generating an earthquake. The *coupled zone* is a proxy for the seismogenic zone and is the part of the plate boundary that has geodetically inferred slip deficit and appears to be storing elastic energy. We define a *rupture patch* as the area on the megathrust that slips during a particular earthquake. We discuss evidence for and against geologically controlled *rupture boundaries* on the megathrust that may define persistent, recurrent rupture patches.

Accurate CSZ megathrust earthquake scenarios hinge on our understanding of the existence and persistence of rupture boundaries, both along-strike and down-dip, and the structural or rheologic properties that modulate these boundaries. Heterogeneities evident in proxies for megathrust behavior may sometimes indicate spatially persistent rupture characteristics like slip or rupture boundaries. We note that potential boundaries do not necessarily inhibit all ruptures, depending on the physics of rupture propagation (Bilek & Lay, 2018). Rupture boundaries may be persistent, frequent, or ephemeral (rarely traversed, occasionally traversed, or always changing, respectively; Philibosian & Meltzner, 2020). For example, the Kii Peninsula in Japan is a boundary along the Nankai-Suruga Trough that impeded throughgoing rupture of the 1944 Tonankai and 1946 Nankai earthquakes, but the 1707 Hoei earthquake ruptured the entire margin (Garrett et al., 2016). While the 1700 CE event in Cascadia was likely an ~M9 earthquake that ruptured the entire length of the CSZ (Atwater et al., 2005), the geologic record likely also preserves smaller earthquakes that only rupture a portion of the subduction zone (Wells et al., 2003; Goldfinger et al., 2012). The long-term persistence of rupture boundaries in Cascadia and elsewhere is an ongoing question (Victor et al., 2011; Meltzner et al., 2012). The geologic record is necessary to verify interpretations of rupture boundaries gleaned from geophysical data, but conversely, along-strike and downdip patterns evident in instrumental datasets may also help distinguish between conflicting interpretations of rupture boundaries the geologic record. Below we summarize the three-dimensional variations in the CSZ environment and megathrust slip behaviors that we can observe with modern geophysical instrumentation.

3.1. Depth-dependent seismic behavior and frictional properties

All subduction zones exhibit depth-dependent slip behaviors along the plate interface (Lay et al., 2012; Bilek & Lay, 2018). In the upper coupled zone, at depths less than ~15 km, strain release generally occurs either largely aseismically or in earthquakes with relatively low amounts of short-period energy radiation and low stress drop (Newman & Okal, 1998; Ye et al., 2016; Sahakian et al., 2019), often termed *tsunami earthquakes* as they generate tsunamis that are anomalously large for the corresponding earthquake magnitude (Hill et al., 2012; Lay et al., 2012). This zone can rupture co-seismically during megathrust earthquakes (e.g., the 2011 M_W 9.0 Tohoku-Oki and 2010 M_W 8.8 Maule events). From ~15-35 km depths, earthquakes can produce large slip and emit broadband seismic waves, although the size of individual rupture patches and amount of slip in each event vary in space and time (Lay et al., 2012; Bilek & Lay, 2018). A transitional zone below ~35 km depth exhibits various types of slow-slip behaviors, including slow-slip events (SSEs) in which several cm of slip occurs over a large area over a period of days-to-years (Obara & Kato, 2016; Bilek & Lay, 2018; Bartlow, 2020). These events occur near where the downgoing plate meets the hydrated mantle wedge (Obara & Kato, 2016; Gao & Wang, 2017). Debates persist over the exact relationships between and physical controls on these depth zones in Cascadia and elsewhere (Obara & Kato, 2016; Wang & Tréhu, 2016; Gao & Wang, 2017).

Limited seafloor geodetic observations and an exceptionally low rate of low-magnitude background interplate seismicity in the CSZ blurs our understanding of the geometry and depth of the seismogenic zone and the degree of interseismic coupling (Wang & Tréhu, 2016). The relative lack of seismicity, along with inversion of geodetic datasets, suggests that the CSZ seismogenic zone is nearly fully coupled along much of its length, although the width and degree of coupling may vary along strike; notably, central Cascadia has been modeled as both an anomalously narrow zone of coupling or a wide zone of partial coupling (Fig. 5; McCaffrey et al., 2013; Schmalzle et al., 2014; Pollitz & Evans, 2017; Li et al., 2018; Michel et al., 2018). Calculated Holocene vertical land motion most closely matches models that include a fully locked CSZ at shallow (<30 km) depths (Fig. 5; Yousefi et al., 2020). In general, the width of the inferred seismogenic zone in Cascadia decreases to the south, potentially impacting

megathrust earthquake slip magnitude, an interpretation that is consistent with the apparent increase in megathrust event frequency from the geologic record (Scholz, 2014; Tréhu, 2016). The recent and planned installation of offshore GNSS-Acoustic (GNSS-A) instrumentation should reduce the non-uniqueness of coupling models by helping to constrain offshore strain accumulation (Bürgmann & Chadwell, 2014; Heesemann et al., 2017; Chadwell et al., 2018; Fig. 5). Initial data from these GNSS-A sites indicates a high degree of near-trench coupling (Chadwell et al., 2018).

Direct observations of earthquakes in other subduction zones inform our understanding of CSZ rupture processes. Ground motion observations from the 2011 M_W 9.0 Tohoku-Oki and 2010 M_W 8.8 Maule events suggest that the frequency content of the radiated seismic energy varies with depth within the seismogenic zone. Ground motions from these two events can be explained by incorporating high-stress-drop *subevents*, which are M8-size rupture patches at 20-30 km depths superimposed on the lower-stress-drop background slip (Wang & Mori, 2011; Frankel, 2013). Recent CSZ ~M9 rupture models include such subevents (Frankel et al., 2018; Wirth et al., 2018) and are compatible with variability in 1700 CE coseismic subsidence estimates (Wirth & Frankel, 2019). Inclusion of modeled high-stress-drop subevents impacts slip patterns, ground motions, upper plate structure, and interpretation of ground shaking proxies in the geologic record, although their full impact requires further investigation. Shallow (depths less than ~10-15 km) tsunami earthquakes typically exhibit much weaker shaking (Sahakian et al., 2019). The resulting slip distribution and seafloor deformation from shallow earthquakes is also a critical control on coseismic hazards, specifically tsunami inundation (Priest et al., 2014; Melgar et al., 2016).

Seismically and geodetically measured slow-slip and tremor phenomena, termed *episodic tremor and slip* (ETS), occurs with remarkable regularity along the CSZ (Fig. 1E; Dragert et al. 2001; Rogers & Dragert, 2003; Brudzinski & Allen, 2007; Gomberg, 2010; Boyarko et al., 2015; Wells et al., 2017; Bartlow, 2020). ETS occurs at ~30-40 km depths below the seismically coupled zone, with a creeping gap between the base of the coupled zone and the slow-slip zone (Hyndman et al., 2015; Bruhat & Segall, 2016; Bartlow, 2020; Fig. 1E). Slow slip and tremor phenomena migrate together, suggesting that these phenomena are different manifestations of the same seismic process (Bartlow et al., 2011). Although we currently do not fully understand the exact physical controls on slow slip and its relationship to geodetic coupling, high pore fluid pressures near the mantle wedge may be responsible for generating slow slip here (Hyndman et al., 2015; Wang & Tréhu, 2016; Gao & Wang, 2017). Globally, SSEs generally occur along megathrust interfaces that have relatively young downgoing oceanic lithosphere (Lay et al., 2012). SSEs do not accommodate the full slip budget along most of the subduction zone, implying significant inter-SSE creep may occur on the interface within the SSE zone (Bartlow, 2020). Whether any slip deficit in this depth range will contribute to slip during a future CSZ megathrust earthquake remains a mystery, and the degree to which stresses from slow-slip events may be important in triggering the next great earthquake in Cascadia is a matter of current debate (Mazzotti & Adams, 2004; Beeler et al., 2014; Bartlow, 2020).

3.2. Along-strike variability in slip behavior and structure

Many geophysical imaging studies in Cascadia indicate that along-strike heterogeneity exists in forearc upper plate crustal structure. For example, the early Eocene-age Siletz/Crescent terrane that forms the crystalline basement throughout much of the Cascadia forearc (Fig. 5) is unusually thick and extends offshore between ~43°and 46°N. The unique composition of this terrane and other crystalline terranes within Cascadia has been correlated with along-strike variations in upper plate seismicity, ETS periodicity and slip, degree of coupling, and other factors (Fig. 5; Tréhu et al., 1994; 2012; Wells et al., 1998, 2003; Brudzinski & Allen, 2007; Porritt et al., 2011; Li & Liu, 2016; Delph et al., 2019; Egbert et al., 2019; Bartlow, 2020). The Siletz terrane exists along the stretch of central Cascadia where geodetic models show a narrow,

fully coupled zone or a wide, partially coupled zone (Fig. 5; Schmalzle et al., 2014). Wells et al. (2017) speculated that upper-plate faults in the brittle Siletz terrane reduce fluid overpressure and de-optimize tremor conditions. In a comprehensive examination of the tectonic geomorphology, outer wedge taper, and seaward and landward structural vergence along the accretionary complex, Watt & Brothers (2020) concluded that along-strike variations in shallow megathrust behavior correlate with upper plate structural boundaries and suggested that the thickened Siletz terrane acts as a backstop influencing the frictional properties of the megathrust through modulation of wedge strength (Figs. 4 & 5).

In the seismogenic zone, model results for 1700 CE slip distribution constrained by land-level change data (Wang et al., 2013) show possible low-slip regions that correlate with structural boundaries located roughly near 42-43°N, 44.5°N, and 46°N (Figs. 4 & 5). The degree of coupling along strike may relate to variation in buoyant asthenosphere beneath the downgoing plate; Bodmer et al. (2018) used seismic tomography to argue for decreased buoyancy of the subducting Juan de Fuca plate between ~43° and 46°N, relating it to decreased interplate coupling and non-volcanic tremor at these latitudes (Figs. 4 & 5). Wells et al. (2003) argued that forearc basins represent basal erosion of the upper plate due to increased frictional strength of the plate boundary, forming potentially recurrent high-slip patches over multiple earthquake cycles (Fig. 5). Stone et al. (2018) found generally higher rates of forearc seismicity south of 46°N and correlate this with incoming plate roughness and sediment thickness (Fig. 5). Persistent clusters of seismicity during the past several decades on or near the plate boundary within the seismogenic zone near 44.3°N and 44.6°N also correlate with subducted seamounts inferred from potential field and seismic imaging data (Figs. 4 & 5; Tréhu et al., 2012, 2015; Morton et al., 2018; Stone et al., 2018). Tréhu et al. (2012) attributed these clusters to interactions between subducted seamounts and the Siletz terrane.

While numerous geophysical and instrumental datasets reveal along-strike variation of the CSZ, the relevance of these observations for understanding the dynamic behavior of past and future CSZ earthquakes is complex and controversial (Philibosian & Meltzner, 2020). Along-strike variations in paleoseismic data (Goldfinger et al., 2017) remain the most direct proxies for past earthquake behavior and to verify boundaries hypothesized from geophysical data. Given the lack of coseismic observations, we cannot immediately resolve the causes for along-strike correlations in geophysical data, and we have limited ability to link inferred changes in frictional properties along the megathrust to slip behavior and long-term strain accumulation patterns in Cascadia. Well-resolved preseismic, coseismic, and postseismic observations on other subduction zones provide a framework for interpreting geophysical and instrumental records in Cascadia. Many studies have modeled and interpreted activity in subduction zone earthquakes in the context of geologic structure (Davis et al., 1983; von Huene & Scholl, 1991; Saffer & Bekins, 2002; Lamb, 2006; Fujie et al., 2013; Cubas et al., 2013; McNeill & Henstock, 2014; Henstock et al., 2016; Bassett et al., 2016; Saillard et al., 2017; Tréhu et al., 2019; Olsen et al., 2020). Comparative studies can help to reconcile geophysical observations with the geologic record to best understand CSZ recurrence.

4. Recurrence models and implications for seismic hazard

A fundamental aim of CSZ paleoseismic studies is to determine a recurrence model that fits our understanding of past CSZ earthquakes. A well-constrained recurrence model is particularly relevant for Probabilistic Seismic Hazard Assessment (PSHA) models, which form the basis for the US National Seismic Hazard Maps (NSHM; Petersen et al., 2019). PSHA models estimate the probability of ground motion exceedance, termed *hazard* (Cornell, 1968), using input earthquake scenarios describing the slip distribution, fault location, fault geometry, and recurrence. Earthquake recurrence models typically considered for subduction zone margins

and other major fault systems are categorized as either time-independent or time-dependent (Table 1).

The time-independent model is a common choice for PSHA models, especially when applied to broad regions with multiple fault systems because it requires minimal information, namely mean recurrence rate. Often described as a Poisson process, time-independence assumes that events occur at a certain mean rate but with random event timing. The time-independent recurrence implies that occurrence is memoryless, hazard is constant, and may suggest that accumulated far-field stress on the fault system does not define earthquake rupture timing (Fig. 6; Table 1). The aggregate behavior of a region may appear Poissonian, even if composed of faults with individually time-dependent earthquake recurrence (Cornell & Winterstein, 1988).

Time-dependent recurrence assumes that earthquakes rupture with a regularity defined by accumulated stress levels on the fault system. In a periodic model, both the interevent time and slip during each event are predictable and earthquake hazard probabilities increase proximal to the mean recurrence time (Fig. 6; Table 1; Shimazaki & Nakata, 1980). Idealization of the periodic model suggests common slip magnitude (Fig. 6; Schwartz & Coppersmith, 1984); however, observations suggest a more flexible definition of the periodic model, with quasi-periodic large ruptures in addition to less periodic moderate events with variable rupture characteristics (Zielke, 2018). The clustered model is a subcategory of time-dependent models in which strain energy balances over multiple seismic events followed by a period of seismic quiescence (Fig. 6; Table 1). Slip rate averaged over multiple earthquake cycles is constant, but fault slip for each event can be variable (Fig. 6). Nested clusters of subduction zone earthquakes are termed *supercycles* (Sieh et al., 2008; Goldfinger et al., 2013b; Herrendörfer et al., 2015; Philibosian & Meltzner, 2020).

In this section, we summarize the methodology and underlying assumptions that differentiate between various recurrence models and, as a thought experiment, we explore the range of recurrence models compatible with interpretations of the paleoseismic record. We highlight the difficulty in distinguishing full-margin from serial ruptures in the geologic record, and discuss the implications for seismic hazard assessment.

4.1. The Coefficient of Variance and its application to the CSZ

An outstanding controversy remains, in which some argue all events in the paleoseismic record are full-margin M9s and others argue that a portion of those events may be a series of smaller M8s that occur in quick succession irresolvable by geochronologic uncertainties (Atwater et al., 2014; Frankel et al., 2015). Additional uncertainty remains about potential rupture barriers and how to handle partial ruptures along the margin, particularly the more frequent ruptures interpreted in southern Cascadia. Below, we explore how these two outstanding uncertainties may affect the Coefficient of Variation (*CV*), a simple statistical metric that researchers commonly use to evaluate proposed recurrence models. While not always inclusive of nuanced detail in long paleoseismic records, *CV* values inform hazard analyses on possible recurrence scenarios and thus provide a basis from which to construct hazard models. The equation for *CV* is as follows:

$$CV = \frac{\sigma_{IT}}{\mu_{IT}}$$

where $\sigma_{IT}$and $\mu_{IT}$are the standard deviation and mean of interevent times, τ, respectively (Cramer et al., 2000; Field, 2015; Table 1). In the time-independent model, random processes lead to similar means and standard deviations, thus the $CV \approx 1$. In the time-dependent periodic model, consistent interevent times result in a small standard deviation and $CV \leq 1$. A $CV \geq 1$ indicates variable interevent times and suggests clustered behavior (Table 1). Application of *CV* assumes a well-sampled seismic catalog that is long enough to capture typical recurrence

behavior. Petersen et al. (2002) evaluated a *CV* between 0.1 and 0.4 for the Pacific Northwest but included crustal and intraplate events; here we focus on the megathrust to discuss the CSZ earthquake cycle model. Recurrence models and the *CV* apply to a catalog of *significant events*, which are fault slip events that release enough stress to permit statistical renewal of the recurrence process. This generally requires a rupture of the full fault system, or a large enough rupture to relieve sufficient accumulated stress (Herrendörfer et al., 2015).

4.2. Full-margin ruptures

Geoscientists infer 19 - 20 full-margin ~M9 CSZ earthquakes over the past 10 kyr from marine and onshore geologic datasets (Goldfinger et al., 2012; 2017; Enkin et al., 2013, Hamilton et al., 2015; Fig. 4). Using this catalog, *CV* calculations imply time-dependent quasi-periodic recurrence in Cascadia (*CV* = 0.51; Tables S3-S4). If partial-margin ruptures longer than 660 km (Table S4) are significant and renew the recurrence process, *CV* reduces to 0.39 (Table S3). These *CV* estimates vary insignificantly regardless of whether we include events with weak onshore geologic support (e.g., T2; Table S3). These basic *CV* calculations strongly suggest a quasi-periodic recurrence model for the CSZ (Table S3), assuming correlated events are single ~M9 ruptures. If correct, the quasi-periodic recurrence model would suggest that the CSZ is currently in the late stages of the earthquake deformation model.

Goldfinger et al. (2012) and Kulkarni et al., (2013) identify temporal gaps after T5, T10, and T15 in the marine record to argue for clustered full-margin event recurrence; however, some onshore events along the margin may fill in these temporal gaps along the margin (e.g., John's River to Lagoon Creek between T5 and T6; Fig. 4). The potential for clustered CSZ megathrust earthquakes has important hazard implications (Kulkarni et al., 2013), and therefore merits attention.

4.3. Serial and partial ruptures

The uncertainty in ^{14}C dating techniques (10s to 100s of years) allows for the possibility of interpreting some of the 19 - 20 correlated events as *serial ruptures*, in which time intervals smaller than dating uncertainties separate multiple ~M8 earthquakes (Fig. 2). Currently, little evidence supports serial rupture as a common seismic occurrence along the CSZ, however two events captured in the Bradley Lake record are separated by >22 years (Kelsey et al., 2005) correlate to a possible T5 turbidite doublet in Rogue Canyon marine cores (Goldfinger et al., 2012), suggesting serial ruptures may occur occasionally. If we assume one third to one half of the full-margin events interpreted by Goldfinger et al. (2012) are actually 3 - 4 serial ruptures separated by 10 - 100 years (Table S4), the resulting *CVs* suggest Poisson and clustered recurrence models, respectively (Table S3). We only consider up to half of events as possible serial ~M8 ruptures, as a majority of ~M9 ruptures are required to accommodate incoming plate convergence rate seismically (Frankel et al., 2015). These hypothetical rupture scenarios indicate that *CV* estimates for non-quasi-periodic recurrence are attainable only if a large portion of the geologic record has been misinterpreted as full-margin M9 ruptures.

In addition to uncertainty in full-margin rupture regularity, portions of the CSZ seem to rupture more frequently and may have an earthquake cycle independent of the full-margin cycle. Some geologic data south of Cape Blanco show a striking increase in the number of events recorded and a corresponding decrease in the interevent time (Fig. 4; Table S3). The marine core record includes 17 additional events, many from mud turbidites, limited to southern Cascadia (Table S3; Goldfinger et al., 2012). Whether these events represent CSZ or crustal earthquakes remains an open question (Goldfinger & Gutierrez, 2019). Onshore records indicate 11 events limited to south of Cape Blanco and two limited to northern Cascadia (Fig. 4; Blais-Stevens et al., 2011; Williams et al., 2005; Nelson et al., 2006). Assuming these smaller ruptures represent CSZ earthquakes, the *CV* applied to southern Cascadia ruptures implies a time-

dependent, quasi-periodic recurrence model (Tables S3-S4). The recurrence interval for ruptures limited to northern Cascadia remains elusive (Petersen et al., 2014).

4.4. Implications for the CSZ earthquake cycle model

Various rupture scenarios discussed above lead to *CV* values consistent with interpretation of Poisson, quasi-periodic, and clustered recurrence models for the CSZ. This highlights how current dating uncertainties and debates on rupture variability along the CSZ render an evaluation of the earthquake cycle model in Cascadia premature.

PSHA offers a means of quantifying the intrinsic variability of the system, termed *aleatoric variability,* and addressing uncertainties that stem from limited knowledge, termed *epistemic uncertainty*. The current U.S. NSHM uses extensive logic trees that weigh various M8 and M9 rupture scenarios to define two additive CSZ earthquake scenarios: (1) full margin ~M9 that recur every ~500 years and (2) partial M8.0-8.7 rupture of the CSZ (Frankel et al., 2015). The recurrence rates for partial ruptures in northern and southern Cascadia, which strongly influence hazard, are averaged between different possible scenarios supported by onshore or offshore evidence (Petersen et al., 2014; Frankel et al., 2015). Future updates to the U.S. NSHM may include the possibility of serial rupture (Frankel et al., 2015). Accurate hazard analyses can improve by reducing epistemic uncertainty (Sykes & Menke, 2006), which can only be addressed with further geologic and geophysical research.

5. Future research directions

Decades of research have led to enviable geologic datasets that record past megathrust earthquakes in Cascadia as well as diverse geophysical observations along the margin. However, major outstanding questions on earthquake occurrence and rupture characteristics remain. In this section, we highlight knowledge gaps, discrepancies between datasets, and uncertainties in earthquake recurrence that may be addressed through collection of new data, careful integration of available datasets, and consideration of the processes that created the records we observe today in Cascadia.

5.1. Outstanding knowledge gaps in CSZ earthquake characteristics and recurrence

Discrepancies in onshore and offshore geologic evidence for megathrust rupture currently fuel ambiguity in records of megathrust recurrence. Paleoseismic events recorded in the marine record do not all share a corresponding record on land (Fig. 4). Mismatch between the datasets is at least partly due to variable evidence thresholds and analytical uncertainties inherent in geochronology (Nelson et al., 2006), but additionally, the geochronologic age corrections applied to onshore and offshore datasets differ, causing difficulty in correlation.

The magnitude of past earthquake events is also difficult to resolve from geologic datasets. Current dating methods and models for CSZ events recorded at individual sites along the margin also have enough uncertainty that experts continue to debate whether full-margin events are always single ~M9 events or if some small portion might be multiple successive M8 events (Fig. 2C; Petersen et al., 2014). Without Japanese tsunami records and modeling, it is difficult to distinguish the 1700 CE earthquake as a single ~M9 or multiple ~M8s. Both paleoseismic and geophysical datasets hint at potentially persistent rupture barriers along the CSZ margin, but it is unclear which barrier proxies are most relevant for understanding coseismic rupture processes. The presence and persistence of rupture barriers may also cause the earthquake cycle model to vary along the megathrust, and the possibility that some past earthquakes were shallow tsunami earthquakes also contributes to uncertainty (Tréhu, 2016).

Other aspects of coseismic rupture processes remain elusive. For instance, current geodetic coverage does not uniquely resolve coupling on the subduction zone interface. Without an instrumental record of a great CSZ megathrust earthquake, estimating coseismic onshore and offshore ground motion and secondary hazards, such as liquefaction, landslides, and turbidites,

often relies on comparison to other subduction zone margins. The limited liquefaction and landslide evidence for the 1700 CE earthquake inhibits accurately estimating local and regional ground motion for future events. Additionally, numerous assumptions underpin current understanding of shaking-initiated sediment transport processes in the CSZ; we currently lack clarity on how, and under what conditions, the geologic record archives various shaking proxies.

Due to the gaps in knowledge, there is currently no consensus on an appropriate recurrence model for the CSZ. For recurrence estimates, questions remain about the magnitude threshold required to constitute a significant event, and whether CSZ geologic records capture all significant earthquakes. Some geologic records may record events <M8, or record events caused by other earthquake sources, such as the northern San Andreas fault. Defining a recurrence model and understanding the physical processes influencing recurrence also requires that the geologic record spans enough time to statistically capture potential variability.

5.2. Future research directions in CSZ science

Geologic records at the CSZ still present multiple opportunities for advancement. New paleoseismic sites that capitalize on potential for longer temporal records will allow for further exploration of the extent of past megathrust rupture and help identify variability in rupture characteristics. Filling latitudinal spatial gaps in land-level change records may improve recurrence and rupture models (Fig S1). In addition to study of new locales, modern methodology and statistical analyses can help to reduce uncertainty in available datasets.

New Bayesian transfer functions that can incorporate multiple microfossil proxies reduce uncertainties on subsidence estimates (Kemp et al., 2018), and applying this method downcore can resolve slip over multiple earthquake cycles, improving our knowledge of slip along the megathrust through time and space (Padgett et al., in review). Microfossil-based analyses also have the potential to quantify interseismic (Shennan et al., 1999) and postseismic (Horton et al., 2017) deformation, but constraining the age of the inorganic tidal mud that accumulates in the postseismic and interseismic periods remains a challenge. At previously investigated locales along the coast (Fig. S1), widespread, precise quantitative microfossil-based estimates of coseismic subsidence in 1700 CE have informed heterogenous rupture models; however, limited and imprecise subsidence estimates for older events do not resolve slip along the megathrust at a high-enough resolution to differentiate uniform and heterogenous model solutions (Leonard et al., 2010; Milker et al., 2016).

Existing uncertainties in dating earthquake events remains one of the largest barriers to reducing the nonuniqueness of geologic correlations and interpretations (Hutchinson & Clague, 2017). Dendrochronology offers sub-annual temporal resolution of land-level changes, and while such resolution still cannot discriminate between serial partial-margin ruptures separated by days or months from single full-margin earthquakes, confidence in the interpretation could improve significantly. Modern dendrochronology methods utilize changes in wood chemistry that may accompany sudden coseismic subsidence (Pearl et al., 2020a) and known spikes in the radiocarbon record as chronologic tie points (Pearl et al., 2020b, Pearson et al., 2020). Dendrochronology could also assist with dating landslide-dammed lakes (Struble et al., 2020). Bayesian age-modeling of detrital macrofossil radiocarbon dates provides another promising approach to reduce uncertainties that has only been newly applied in Cascadia (Nelson et al., 2020; Padgett et al., in review). Offshore, turbidite ages may improve by using more standardized calibrations and reservoir corrections (Clark et al., 2019).

Geodetic models and the near absence of seismicity on the megathrust since the 1700 CE earthquake are consistent with coupling of the CSZ plate boundary to at least some degree (Schmalzle et al. 2014; Wang & Tréhu, 2016), but offshore geodetic data are critical for obtaining high-resolution spatial constraints on the degree of coupling and reducing the number of viable coupling models (Bürgmann & Chadwell, 2014). Twelve seafloor GNSS-A stations have been deployed on the Juan de Fuca and North American plates since 1991, most in the past

few years. Sites on the North American plate near the trench measure shallow coupling (Fig. 5; Bürgmann & Chadwell, 2014; Heesemann et al., 2017; Chadwell et al., 2018). Researchers plan to deploy at least two more sites on and near the Gorda plate (Fig. 5), which features significant internal deformation that is currently poorly constrained (Bartlow, 2020). Comparison of the CSZ with other instrumentally monitored subduction zones, such as Nankai (Kano & Kato, 2020), can offer clues to the state of coupling, unusual paucity of interplate CSZ seismicity, and the role of slow slip in the accommodation of convergence (Wang & Tréhu, 2016; Bartlow, 2020).

New structural imaging will also improve definition of potential along-strike rupture boundaries, allowing for better correlations between structure and dynamic behavior of the CSZ. Acquisition of high-resolution offshore imagery and sediment cores across Cascadia's deformation front, combined with quantitative modeling of tsunami generation and sediment transport, will better inform interpretations of tsunami deposits left behind from past earthquakes. Future efforts may also focus on determining whether or not there is on-fault marine geologic evidence of near-trench rupture along the Cascadia deformation front and the role of splay faults in tsunamigenic rupture (Fig. 1D; Beeson et al., 2017).

Broadening the spatial extent of shaking proxy datasets, such as landslides, liquefaction, lacustrine turbidites, and marine turbidites could substantially improve estimates of past earthquake ground motion. Repeat high-resolution bathymetric mapping and subsurface imaging offer promising techniques to test assumptions made in interpretation of mass-transport deposits (Mountjoy et al. 2018; Hill et al., 2020). Shaking from earthquakes along non-megathrust crustal faults can complicate interpretation of the geologic record (Clark et al., 2019), though systematic examination of this process along the CSZ has yet to happen and may be an important avenue for future investigation. To this end, lacustrine paleoseismology offers exciting new research avenues to address onshore ground motions for past megathrust events (Morey et al., 2013, Goldfinger et al., 2016), as well as to improve crustal and intraplate earthquake catalogs (van Daele et al., 2019).

5.3. An integrative concept for CSZ science

To address and potentially resolve discrepancies and uncertainties in the geologic data, we suggest that future work applies an integrative approach that considers different evidence thresholds of geologic datasets, proxies for megathrust behavior, and potential rupture barriers gleaned from geophysical and instrumental datasets to provide more accurate estimates of past earthquake rupture characteristics.

We can leverage differences in evidence thresholds to learn more about the preservation of earthquake processes in the geologic record. An example from southern Oregon illustrates these thresholds, where Bradley Lake preserves evidence for 12 megathrust-generated tsunami deposits in the past 5000 years (Kelsey et al., 2005), while nearby subsidence records only show 9 or 10 events in the same time period (Kelsey et al., 2002; Witter et al., 2003). Similarly, while onshore records also suggest a greater number of earthquakes in southern Cascadia (Nelson et al., 2006), not all turbidite events have a corresponding record on land (Fig. 4). These records may suggest that for some CSZ ruptures, turbidite and/or tsunami deposits are more likely to be created and preserved in southern Cascadia compared to land-level change (Nelson et al., 2006).

Rupture patch location, extent, and slip magnitude likely bear on evidence threshold, as different rupture properties can generate particular secondary effects. For instance, shallow rupture near the trench may cause sufficient seafloor deformation and ground shaking of the accretionary wedge to create tsunamis and turbidites, respectively. The potential for tsunami earthquakes can alter our interpretation of the geologic record and are relevant to consider for structural interpretation. A shallow tsunami earthquake can produce tsunami deposits in a large region indicative of a M8-M9 event, but in fact come from a smaller M7-M8 event (Hill et al., 2012). Tsunami earthquakes also emit limited high-frequency energy and thus may produce

little to no shaking proxies in the geologic record (Newman & Okal, 1998; Ye et al., 2016; Sahakian et al., 2019). Integration and careful consideration of the available geologic datasets may therefore enable better mapping of past earthquake extent and estimates of rupture characteristics.

Numerous geophysical datasets provide information about the state of coupling, seismicity, and structure along the CSZ, but interpretations disagree, and models provide non-unique solutions. Systematic and analytical comparisons between geophysical, structural, and modeling datasets both within the CSZ and with other subduction zone margins could assist with better understanding the likelihood of potential rupture barriers and other rupture processes. For example, Wang & Tréhu (2016) note the potential for comparing the offshore morphology and structure of the CSZ accretionary complex to other subduction zone margins that have undergone trench-breaching slip (e.g., 2011 Mw 9.0 Tohoku event; Fujiwara et al., 2011).

Inferred relationships between ground motions and shaking-induced sediment transport require rigorous testing, particularly with respect to submarine and terrestrial slope stability, the shear strength of slope sediments, and turbidity flow triggering. New monitoring systems offer *in situ* observations of shaking and how the sediment structure affects site-specific response to ground motion (Gomberg et al., 2019; Jibson et al., 2004). The distributions of landslides across the landscape in response to ground shaking is often complex and thus difficult to characterize and link to earthquake triggers (Struble et al., 2020; LaHusen et al., in press). With improved understanding of the relationship between seismic shaking and site properties, there is potential to identify the influence of megathrust earthquake shaking on terrestrial landslides (Meunier et al., 2007, 2013) by comparing landslide catalogs (Jones et al., 2019) with modeled ~M9 seismic ground-motions (Frankel et al., 2018; Wirth et al., 2018). Compilation of liquefaction data along the CSZ can also improve shaking estimates in areas with sparse geologic proxies.

The CSZ margin is primed for quantitative and inclusive comparisons of proposed rupture boundaries and characteristics with geologic datasets (Figs. 4 & 5). Clark et al. (2019) integrated complex and disparate datasets to identify the sources and extents of paleoearthquakes along the Hikurangi margin in New Zealand. Given the extensive geologic data in Cascadia, much of which is more clearly associated with megathrust rupture, a similar approach may be explored along the CSZ. Integration of onshore and offshore geologic records requires uniform treatment of geochronologic datasets, possibly using a Bayesian framework (Clark et al., 2019) that builds upon the recent use and testing of local-scale Bayesian age models (Goldfinger et al., 2014; Nelson et al., 2020; Padgett et al., in review), as well as identification, and ideally quantification, of evidence thresholds for different record types, with the overarching goal of reducing non-unique fit of past rupture scenarios to the geologic record. The addition of abundant geophysical and instrumental records in Cascadia provides prior knowledge of along-strike heterogeneity that will frame the integration of geologic datasets with constraints from numerical and theoretical modeling (Kemp et al., 2018). A comprehensive catalog of past CSZ megathrust rupture scenarios would provide concrete input for PSHA and may identify specific regions most susceptible to subduction zone earthquakes and associated hazards.

Figure Captions

Figure 1. (A) Oblique view of the northwest margin of North American, where the Juan de Fuca and Explorer oceanic plates subduct beneath the North American plate. On the side view, the thin red line between the two tectonic plates represents the region where great earthquakes occur. On the map overlay, the toothed blue line represents the surface trace of the where the subducting plate begins its descent. Major cities are shown as green dots. The purple swath shows the general region where episodic tremor and slip (ETS) occurs and the pink swath shows the general region considered to be the coupled zone. To the left and below (A), small diagrams illustrate various earthquake-related processes labeled beneath each diagram: (B) coseismic

turbidite generation, (C) coseismic subsidence with dotted green line showing the pre-event coastal land-level, dead brown trees represent marine incursion onto a formerly terrestrial environment (D) and tsunami generation, (E) the relationship between the coupled fault and the ETS zone, with an ETS swarm depicted as blue circles, with a possible gap between the coupled zone and updip extent of ETS shown as a gradational area (F) coseismic landslide hazards, with schematic seismograms (in blue) showing the potential for topographic effects on ground motion amplification, and (G) how geologic features, such as sedimentary basins, can amplify seismic waves.

Figure 2. (A) Block diagram of the interseismic period, when convergence along the coupled subduction zone interface (red zone) typically causes gradual uplift in the onshore overriding plate, and gradual subsidence offshore. (B) Diagram of the coseismic period, when earthquake rupture along the subduction zone interface relieves accumulated strain and generally causes sudden subsidence in the onshore overriding place and sudden uplift in the offshore overriding plate. Shallow rupture may generate a tsunami. (C) Possible scenarios for an ~M9 (orange) and ~M8 (blue) events that rupture the CSZ plate interface. (D) Schematic diagrams of stratigraphic evidence for the earthquake deformation cycle. Left column shows the effect of coseismic subsidence on wetland stratigraphy and coastal forests and their preservation in the stratigraphic record (see also Fig. 1C). Right column shows stratigraphic preservation of coseismic tsunami deposits and liquefaction injectites.

Figure 3. (A) Evidence for coseismic subsidence and tsunami inundation from a sedimentary exposure of subaerial dune sand and prehistoric settlements overlain by tsunami sand and tidal mud along the Salmon River, Oregon (Atwater et al., 2005). (B) Coseismic subsidence evidence from a drowned tree stump surrounded by tidal mud in the Naselle River near Willapa Bay, Washington (Atwater et al., 2005). (C) Marine sediment core showing dark bands of sandy sediment, interpreted as coseismic turbidite deposits, interbedded with lighter colored hemipelagic clay (photograph by C. Goldfinger). (D) An example of a coseismic landslide that dammed a river to produce a "quake lake," from the 1976 Guatemala earthquake (Espinosa, 1976). While not an example of coseismic landsliding in Cascadia, this photo demonstrates secondary hazard potential to the Pacific Northwest.

Figure 4. (Left) Onshore and offshore geologic evidence for CSZ megathrust rupture. Semi-transparent green and blue horizontal bars indicate the temporal length of each record. Onshore and offshore event age range estimates are color-coded with site location (map figure to the right). Offshore age ranges are from turbidites analyzed by Goldfinger et al., 2012. Thick horizontal age ranges are sandy marine turbidite ages estimated from ^{14}C dating of hemipelagic sediments, estimated basal erosion, and inferred sedimentation rate for each geographic locale. Thin horizontal age ranges are calculated ages of interbedded hemipelagic sediment. All age ranges are 2σ uncertainty propagated through ^{14}C age calibration and correction. Vertical grey bars are interpreted event ages from a land-marine age compilation, which takes several onshore geology sites into account with some, but not all, of the geochronologic and stratigraphic information from marine sediment cores (Goldfinger et al., 2012; Table S1). The shade of grey reflects the number of onshore sites plotted here that are consistent with this interpretation (darker = more overlapping onshore data). Age ranges for onshore geologic evidence shown with hatched fill. Age ranges for subsidence (white arrow) and/or tsunami deposit (cute little wave) events are calibrated ^{14}C dates or from OxCal modeling. GF2012 refers to Goldfinger et al. (2012). (Middle) Map shows the locations of onshore and offshore study sites, colored location markers correlate with the age-range panel to the left. Offshore canyons labeled using white text with colored outlines that correlate with turbidite age range bars determined for turbidites associated with that canyon. Black text outlines denote canyon data lacking or not

used. Core ID numbers are available in Figure S1. Marine cores shown are only those used for age dating or stratigraphic correlation; additional marine core locations are in Goldfinger et al., 2012. Nearshore geographic features labeled in purple. Onshore geographic features labeled in blue. Bathymetric contours are 100 meter spacing in light grey, 500 meter interval in dark grey (derived from Wong & Grim, 2015). (Right) North-south evidence for possible rupture boundaries inferred from geophysical datasets, adapted from Watt & Brothers (2020). Circles denote locations of observations of along-strike heterogeneities. Latitudes correspond to the map.

Figure 5. Maps of geophysical and geologic datasets used to infer along-strike heterogeneities along the CSZ. Left map shows heterogeneities on the incoming plate and plate interface. Time-averaged ETS slip rates from Bartlow (2020) are shown as contours with values from 30, 10, and 1 mm/yr. Seismicity from Stone et al. (2018) shows events associated with the CSZ, though note that earthquake depths are poorly constrained and some events may be located within the upper plate. Dense clusters of seismicity near latitudes 44.3° and 44.6° are coincident with subducted seamounts interpreted from magnetic and gravity anomalies (Trèhu et al., 2012). Right map shows heterogeneities on the overriding plate. Morphotectonic zones inferred do not necessarily have sharp boundaries (Watt & Brothers, 2020). VLM: Vertical Land Motion. Fault and lineament names: LR—Leech River fault; S—Seattlefault; SWI—South Whidbey Island fault; LCBC—Lake Creek Boundary Creek fault; DO—Doty fault; CR—Columbia River fault; GC—Gales Creek fault; TY—Tillamook-Yamhill fault; CO—Corvallis fault; WS—Wildlife Safari fault; CV—Canyonville fault; KR—Klamath River lineament; PH–Portland Hills fault; BC—Battle Creek fault. Bathymetric baselayer from Wong & Grim, 2015).

Figure 6. Schematic depiction of recurrence models often proposed for subduction zone settings. (A) Time-dependent model suggests periodic earthquake occurrence is dependent on steady long-term strain accumulation and failure at a critical stress level (i.e., from σ_O to σ_F). This model suggests predictable slip magnitude. (B) Clustered time-dependent model suggests earthquake recurrence is variable, with clustered occurrence earthquakes punctuated by longer intervals, τ_B, of seismic quiescence. Within a cluster, the probability of recurrence at return-interval of τ_A is high. Following a cluster, probability of recurrence decreases until the onset of the next cluster at return interval of τ_B. This model suggests long-term strain accumulation and slip rate may be similar to the periodic model but that slip and timing is less predictable. (C) Time-independent models suggest that earthquake occurrence is unpredictable and may indicate that the displacement rate at the fault trace averaged over several consecutive earthquakes is non-linear.

Acknowledgments
This work was conducted as a part of the "Margin-wide geological and geophysical synthesis to understand the recurrence and hazards of great subduction zone earthquakes in Cascadia" project supported by the U.S. Geological Survey John Wesley Powell Center for Analysis and Synthesis. We thank the numerous scientists who contributed to our Powell Center working group meetings and consulted on or reviewed the content of this paper. We especially thank Art Frankel, Alex Grant, Ruth Harris, Charlie Paull, and Richard Styron for their participation in this project, and the Powell Center leadership team, particularly Jill Baron and Leah Colasuonno. Thanks to Rich Briggs and an anonymous reviewer for their constructive feedback. Any use of trade, product, or firm names is for descriptive purposes only and does not imply endorsement by the U.S. Government.

Literature Cited

Adams J. 1990. Paleoseismicity of the Cascadia Subduction Zone: Evidence from turbidites off the Oregon-Washington Margin. Tectonics. 9(4):569–83.

Atwater BF. 1994. Geology of Holocene Liquefaction Features Along the Lower Columbia River At Marsh, Brush, Price, Hunting, and Wallace Islands, Oregon and Washington. United States Geological Survey Open File Report 94-209.

Atwater BF, Griggs GB. 2012. Deep-Sea Turbidites as Guides to Holocene Earthquake history at the Cascadia Subduction Zone: Alternative Views for a Seismic-Hazard Workshop. US Geological Survey.

Atwater BF, Hemphill-Haley E. 1997. Recurrence Intervals for Great Earthquakes of the Past 3,500 Years at Northeastern Willapa Bay, Washington. United States Geol. Surv. Prof. Pap.

Atwater BF, Yamaguchi DK. 1991. Sudden, probably coseismic submergence of Holocene trees and grass in coastal Washington State. Geology. 19(7):706–9.

Atwater BF, Musumi-Rokkaku S, Satake K, Tsuji Y, Ueda K, Yamaguchi DK. 2005. The Orphan Tsunami of 1700. Reston, Virginia. US Geol. Surv. Univ. Washingt. Press. Seattle, Washingt. 133pp.

Atwater, BF, Carson B, Griggs GB, Johnson HP, Salmi MS. 2014. Rethinking turbidite paleoseismology along the Cascadia subduction zone. Geology. 42(9), 827-830.

Bartlow NM, Miyazaki S, Bradley AM, Segall P. 2011. Space-time correlation of slip and tremor during the 2009 Cascadia slow slip event. Geophys. Res. Lett. 38(18):1-6.

Bartlow NM. 2020. A Long-Term View of Episodic Tremor and Slip in Cascadia. Geophys. Res. Lett. 47(3):1–9.

Bassett D, Sandwell DT, Fialko Y, Watts AB. 2016. Upper-plate controls on co-seismic slip in the 2011 magnitude 9.0 Tohoku-oki earthquake. Nature. 531(7592):92–96.

Beeler NM, Roeloffs E, McCausland W. 2014. Re-estimated effects of deep episodic slip on the occurrence and probability of great earthquakes in Cascadia. Bull. Seismol. Soc. Am. 104(1):128-44.

Beeson JW, Goldfinger C, Fortin WF. 2017. Large-scale modification of submarine geomorphic features on the Cascadia accretionary wedge caused by catastrophic flooding events. Geosphere. 13(5):1713-28.

Bilek SL, Lay T. 2018. Subduction zone megathrust earthquakes. Geosphere. 14(4):1468–1500.

Blais-Stevens A, Rogers GC, Clague JJ. 2011. A revised earthquake chronology for the last 4,000 years inferred from varve-bounded debris-flow deposits beneath an inlet near Victoria, British Columbia. Bull. Seismol. Soc. Am. 101(1):1–12.

Bodmer M, Toomey DR, Hooft EEE, Schmandt B. 2018. Buoyant Asthenosphere Beneath Cascadia Influences Megathrust Segmentation. Geophys. Res. Lett. 45(14):6954–62.

Boyarko DC, Brudzinski MR, Porritt RW, Allen RM, Tréhu AM. 2015. Automated detection and location of tectonic tremor along the entire Cascadia margin from 2005 to 2011. Earth Planet. Sci. Lett. 430:160–70.

Brudzinski MR, Allen RM. 2007. Segmentation in episodic tremor and slip all along Cascadia. Geology. 35(10):907–10.

Bruhat L, Segall P. 2016. Coupling on the northern Cascadia subduction zone from geodetic measurements and physics-based models. J. Geophys. Res. 121(11):8297-314.

Bürgmann R, Chadwell D. 2014. Seafloor Geodesy. Annu. Rev. Earth Planet. Sci. 42:509–34.

Chadwell CD, Schmidt DA, Webb SC, Nooner SL, Ericksen TL, et al. 2018. Expansion of GPS-Acoustic Arrays offshore the Cascadia and Alaska Subduction Zones. In AGU Fall Meeting Abstracts.

Clague JJ, Bobrowsky PT, Hutchinson I. 2000. A review of geological records of large tsunamis at Vancouver Island, British Columbia, and implications for hazard. Quat. Sci. Rev. 19(9):849–63.

Clark K, Howarth J, Litchfield N, Cochran U, Turnbull J, et al. 2019. Geological evidence for past large earthquakes and tsunamis along the Hikurangi subduction margin, New Zealand. Mar. Geol. 412(March):139–72.

Cornell CA, Winterstein SR. 1988. Temporal and magnitude dependence in earthquake recurrence models. Bull. Seismol. Soc. Am. 78(4):1522–37.

Cornell CA. 1968. Engineering seismic risk analysis. Bull. Seismol. Soc. Am. 58(5):1583–1606.

Cramer CH, Petersen MD, Cao T, Toppozada TR, Reichle M. 2000. A Time-Dependent Probabilistic Seismic-Hazard Model for California. Bull. Seismol. Soc. Am. 90(1):1–21.

Cubas N, Avouac JP, Souloumiac P, Leroy Y. 2013. Megathrust friction determined from mechanical analysis of the forearc in the Maule earthquake area. Earth Planet. Sci. Lett. 381(February 2010):92–103.

Darienzo ME, Peterson CD, Clough C. 1994. Stratigraphic evidence for great subduction-zone earthquakes at four estuaries in northern Oregon, USA. J. Coast. Res. 850–76.

Davis D, Dahlen FA, Suppe J. 1983. Mechanics of fold-and-thrust belts and accretionary wedges Cohesive Coulomb theory. J. Geophys. Res. 88(B2):1153–72.

Dragert H, Wang K, James TS. 2001. A silent slip event on the deeper Cascadia subduction interface. Science. 292(5521):1525–28.

Dura T, Engelhart SE, Vacchi M, Horton BP, Kopp RE, et al. 2016a. The Role of Holocene Relative Sea-Level Change in Preserving Records of Subduction Zone Earthquakes. Curr. Clim. Chang. Reports. 2(3):86–100.

Dura T, Hemphill-Haley E, Sawai Y, Horton BP, 2016b. The application of diatoms to reconstruct the history of subduction zone earthquakes and tsunamis. Earth-Science Reviews. 1;152:181-97.

Engelhart SE, Vacchi M, Horton BP, Nelson AR, Kopp RE. 2015. A sea-level database for the Pacific coast of central North America. Quat. Sci. Rev. 113(78–92).

Enkin RJ, Dallimore A, Baker J, Southon JR, Ivanochko T. 2013. A new high-resolution radiocarbon Bayesian age model of the Holocene and Late Pleistocene from core MD02-2494 and others, Effingham Inlet, British Columbia, Canada; with an application to the paleoseismic event chronology of the Cascadia Subduction Zone. Can. J. Earth Sci. 50(7):746–60.

Espinosa AF. 1976. The Guatemalan Earthquake of February 4, 1976. US Geol. Surv. Prof. Pap. 1002:90.

Field EH. 2015. Computing elastic-rebound-motivated earthquake probabilities in unsegmented fault models: A new methodology supported by physics-based simulators. Bull. Seismol. Soc. Am. 105(2):544–59.

Frankel A. 2013. Rupture history of the 2011 M 9 Tohoku Japan earthquake determined from strong-motion and high-rate GPS recordings: Subevents radiating energy in different frequency bands. Bull. Seismol. Soc. Am. 103(2 B):1290–1306.

Frankel A, Chen R, Petersen M, Moschetti M, Sherrod B. 2015. 2014 Update of the Pacific Northwest Portion of the U.S. National Seismic Hazard Maps. Earthq. Spectra. 31(1_suppl):S131–48.

Frankel A, Wirth E, Marafi N, Vidale J, Stephenson W. 2018. Broadband Synthetic Seismograms for Magnitude 9 Earthquakes on the Cascadia Megathrust Based on 3D Simulations and Stochastic Synthetics, Part 1: Methodology and Overall Results. Bull. Seismol. Soc. Am. 108(5A):2347–69.

Fujie G, Kodaira S, Yamashita M, Sato T, Takahashi T, Takahashi N. 2013. Systematic changes in the incoming plate structure at the Kuril trench. Geophys. Res. Lett. 40(1):88–93.

Fujiwara T, Kodaira S, No T, Kaiho Y, Takahashi N, Kaneda Y. 2011. The 2011 Tohoku-Oki earthquake: Displacement reaching the trench axis. Science. 334(6060):1240.

Gao X, Wang K. 2017. Rheological separation of the megathrust seismogenic zone and episodic tremor and slip. Nature. 543(7645):416-419.

Garrett E, Fujiwara O, Garrett P, Heyvaert VMA, Shishikura M, et al. 2016. A systematic review of geological evidence for Holocene earthquakes and tsunamis along the Nankai-Suruga Trough, Japan. Earth-Science Rev. 159:337–57.

Garrison-Laney C, Miller I. 2017. Tsunamis in the Salish Sea: Recurrence, sources, hazards. GSA F. Guid. 49(04):67–78.

Gavey R, Carter L, Liu JT, Talling PJ, Hsu R, et al. 2017. Frequent sediment density flows during 2006 to 2015, triggered by competing seismic and weather events: Observations from subsea cable breaks off southern Taiwan. Mar. Geol. 384:147–58.

Geist EL. 2002. Complex earthquake rupture and local tsunamis. J. Geophys. Res. 107(B5).

Geist EL. 2005. Rapid tsunami models and earthquake source parameters: Far-field and local applications. ISET J. Earthq. Technol. 42(4):127–36.

Goff J, Bobrowsky P, Huntley D, Sawai Y, Tanagawa K. 2020. Palaeotsunamis along Canada's Pacific coast. Quat. Sci. Rev. 237:106309.

Goldfinger C, Kulm LD, McNeill LC, Watts P. 2000. Super-scale failure of the southern Oregon Cascadia margin. Pure Appl. Geophys. 157(6–8):1189–1226.

Goldfinger C, Nelson CH, Morey AE, Johnson JE, Patton JR, et al. 2012. Turbidite Event History — Methods and Implications for Holocene Paleoseismicity of the Cascadia Subduction Zone. US Geological Survey Professional Paper 1661-F.

Goldfinger C, Morey AE, Black B, Beeson J, Nelson CH, et al. 2013a. Spatially limited mud turbidites on the Cascadia margin: Segmented earthquake ruptures? Nat. Hazard Earth Sys. 13(8):2109.

Goldfinger C, Ikeda Y, Yeats RS, Ren J. 2013b. Superquakes and supercycles. Seismol. Res. Lett. 84(1):24–32.

Goldfinger C. 2014. Integrating onshore and offshore paleoseismic data: A Bayesian model. Geological Society of America Annual Meeting, Vancouver British Columbia, October 19-22, 2014.

Goldfinger C, Wong I, Kulkarni R, Beeson JW. 2016. Reply to "Comment on 'Statistical Analyses of Great Earthquake Recurrence along the Cascadia Subduction Zone'". Bull. Seismol. Soc. Am. 106(6):2935-44.

Goldfinger C, Hausmann RB, Black B, Romsos CG, Beeson JW, et al. 2016. Estimating Inland Ground Motions from Lake Turbidite Sequences, Northern Cascadia margin, USA. AGU Fall Meet. Abstr. 2016:T41B-2913

Goldfinger C, Galer S, Beeson J, Hamilton T, Black B, et al. 2017. The importance of site selection, sediment supply, and hydrodynamics: A case study of submarine paleoseismology on the northern Cascadia margin, Washington USA. Mar. Geol. 384:4–46.

Goldfinger C, Gutierrez J. 2019. Possible Stratigraphic Evidence of Stress Triggering of the Northern San Andreas Fault Following Southern Cascadia Earthquakes. AGUFM. 2019:OS54A-03.

Gomberg J. 2010. Slow-slip phenomena in Cascadia from 2007 and beyond: A review. GSA Bull. 122(7–8):963–78.

Gomberg JS, Ludwig KA, Bekins B, Brocher TM, Brock JC, et al. 2017. Reducing risk where tectonic plates collide—U.S. Geological Survey subduction zone science plan. Reston, VA.

Gomberg J, Hautala S, Johnson P, Chiswell S. 2019. Separating Sea and Slow Slip Signals on the Seafloor. J. Geophys. Res. Solid Earth. 124(12):13486–503.

Hamilton TS, Enkin RJ, Riedel M, Rogers GC, Pohlman JW, et al. 2015. Slipstream: an early Holocene slump and turbidite record from the frontal ridge of the Cascadia accretionary wedge off western Canada and paleoseismic implications. Can. J. Earth Sci. 52(6):405-30.

Hansen WR. 1965. Effects of the earthquake of March 27, 1964, at Anchorage, Alaska: Chapter A in The Alaska earthquake, March 27, 1964: effects on communities. Washington, DC.

Hawkes AD, Horton BP, Nelson AR, Vane CH, Sawai Y. 2011. Coastal subsidence in Oregon, USA, during the giant Cascadia earthquake of AD 1700. Quat. Sci. Rev. 30(3–4):364–76.

Heesemann M, Wang K, Davis E, Chadwell CD, Nissen E, et al. 2017. Plans for a Northern Cascadia Subduction Zone Observatory. In AGU Fall Meeting Abstracts.

Hemphill-Haley E. 1995. Diatom evidence for earthquake-induced subsidence and tsunami 300 yr ago in southern coastal Washington. Geol. Soc. Am. Bull. 107(3):367–3.

Henstock TJ, McNeill LC, Bull JM, Cook BJ, Gulick SPS, et al. 2016. Downgoing plate topography stopped rupture in the A.D. 2005 Sumatra earthquake. Geology. 44(1):71–74.

Herrendörfer R, Van Dinther Y, Gerya T, Dalguer LA. 2015. Earthquake supercycle in subduction zones controlled by the width of the seismogenic zone. Nat. Geosci. 8(6):471–74.

Hill EM, Borrero JC, Huang Z, Qiu Q, Banerjee P, et al. 2012. The 2010 Mw 7.8 Mentawai earthquake: Very shallow source of a rare tsunami earthquake determined from tsunami field survey and near-field GPS data. J. Geophys. Res.:117(B6).

Hill JC, Watt JT, Brothers DS, Kluesner JW. 2020. Submarine canyons, slope failures and mass transport processes in southern Cascadia. Geol. Soc. London, Spec. Publ. 500:SP500-2019–2169.

Horton BP, Milker Y, Dura T, Wang K, Bridgeland WT, et al. 2017. Microfossil measures of rapid sea-level rise: Timing of response of two microfossil groups to a sudden tidal-flooding experiment in Cascadia. Geology. 45(6):535–38.

Howarth J, Orpin AR, Nodder S, McCleery D, Strachan LJ, et. al. 2018. Calibrating the turbidite paleoseismometer on the Hikurangi margin, New Zealand, using the 2016 Mw7. 8 Kaikoura earthquake. In AGU Fall Meeting Abstracts.

Hutchinson I. 1992. Holocene sea level change in the Pacific Northwest: a catalogue of radiocarbon dates and an atlas of regional sea-level curves. Institute of Quaternary Research, Simon Fraser University.

Hutchinson I, Clague J. 2017. Were they all giants? Perspectives on late Holocene plate-boundary earthquakes at the northern end of the Cascadia subduction zone. Quat. Sci. Rev. 169:29-49.

Hyndman RD, McCrory PA, Wech A, Kao H, Ague J. 2015. Cascadia subducting plate fluids channelled to fore-arc mantle corner: ETS and silica deposition. J. Geophys. Res. 120(6):4344-58.

Jacoby G, Carver G, Wagner W. 1995. Trees and herbs killed by an earthquake ~300 yr ago at Humboldt Bay, California. Geology. 23(1):77–80.

Jacoby GC, Bunker DE, Benson BE. 1997. Tree-ring evidence for an A.D. 1700 Cascadia earthquake in Washington and northern Oregon. Geology. 25(11):999–1002.

Jibson RW, Harp EL, Schulz W, Keefer DK. 2004. Landslides Triggered by the 2002 Denali Fault, Alaska, Earthquake and the Inferred Nature of the Strong Shaking. Earthq. Spectra. 20(3):669–91.

Jones ES, Mirus BB, Schmitt RG, Baum RL, Burns WJ, et al. 2019. Landslide Inventories across the United States. U.S. Geological Survey data release, https://doi.org/10.5066/P9E2A37P.

Kano M, Kato A. 2020. Detailed Spatial Slip Distribution for Short-term Slow Slip Events along the Nankai Subduction Zone, Southwest Japan. J. Geophys. Res. e2020JB019613.

Karlin RE, Holmes M, Abella SEB, Sylwester R. 2004. Holocene landslides and a 3500-year record of Pacific Northwest earthquakes from sediments in Lake Washington. Bull. Geol. Soc. Am. 116(1–2):94–108.

Kelsey HM, Witter RC, Hemphill-Haley E. 2002. Plate-boundary earthquakes and tsunamis of the past 5500 yr, Sixes River estuary, southern Oregon. Bull. Geol. Soc. Am. 114(3):298–314.

Kelsey HM, Nelson AR, Hemphill-Haley E, Witter RC. 2005. Tsunami history of an Oregon coastal lake reveals a 4600 yr record of great earthquakes on the Cascadia subduction zone. Bull. Geol. Soc. Am. 117(7–8):1009–32.

Kemp AC, Cahill N, Engelhart SE, Hawkes AD, Wang K. 2018. Revising estimates of spatially variable subsidence during the A.D. 1700 cascadia earthquake using a bayesian foraminiferal transfer function. Bull. Seismol. Soc. Am. 108(2):654–73.

Kirk R. 2015. Ozette: Excavating a Makah whaling village. University of Washington Press.

Kulkarni R, Wong I, Zachariasen J, Goldfinger C, Lawrence M. 2013. Statistical analyses of great earthquake recurrence along the Cascadia subduction zone. Bull. Seismol. Soc. Am. 103(6):3205–21.

LaHusen SR, Duvall AR, Booth AM, Grant A, Mishkin BA, Montgomery DR, Struble W, Roering JJ, and Wartman J. In press. Rainfall triggers more deep-seated landslides than Cascadia earthquakes in the Oregon Coast Range, USA. Science Advances.

Lamb S. 2006. Shear stresses on megathrusts: Implications for mountain building behind subduction zones. J. Geophys. Res. Solid Earth. 111(B7).

Lay T, Kanamori H, Ammon CJ, Koper KD, Hutko AR, et al. 2012. Depth-varying rupture properties of subduction zone megathrust faults. J. Geophys. Res. Solid Earth. 117(4):1–21.

Leithold EL, Wegmann KW, Bohnenstiehl DR, Smith SG, Noren A, O'Grady R. 2018. Slope failures within and upstream of Lake Quinault, Washington, as uneven responses to Holocene earthquakes along the Cascadia subduction zone. Quat. Res. (United States). 89(1):178–200.

Leithold EL, Wegmann KW, Bohnenstiehl DR, Joyner CN, Pollen AF. 2019. Repeated megaturbidite deposition in Lake Crescent, Washington, USA, triggered by Holocene ruptures of the Lake Creek-Boundary Creek fault system. Bull. Geol. Soc. Am. 131(11–12):2039–55.

Leonard LJ, Hyndman RD, Mazzotti S. 2004. Coseismic subsidence in the 1700 great Cascadia earthquake: Coastal estimates versus elastic dislocation models. Geol. Soc. Am. Bull. 116(5-6):655-70.

Leonard LJ, Currie CA, Mazzotti S, Hyndman RD. 2010. Rupture area and displacement of past Cascadia great earthquakes from coastal coseismic subsidence. Bull. Geol. Soc. Am. 122(11–12):2079–96.

Li D, Liu Y. 2016. Modeling slow-slip segmentation in Cascadia subduction zone constrained by tremor locations and gravity anomalies. J. Geophys. Res. Solid Earth. 122(4):3138–57.

Li S, Wang K, Wang Y, Jiang Y, Dosso SE. 2018. Geodetically inferred locking state of the Cascadia megathrust based on a viscoelastic Earth model. Journal of Geophysical Research: Solid Earth, 123, 8056–8072.

Long AJ, Shennan I. 1998. Models of rapid relative sea-level change in Washington and Oregon, USA. The Holocene. 8(2):129–42.

Mazzotti S, Adams J. 2004. Variability of near-term probability for the next great earthquake on the Cascadia subduction zone. Bull. Seismol. Soc. Am. 94(5):1954-9.

McCaffrey R, King RW, Payne SJ, Lancaster M. 2013. Active tectonics of northwestern U.S. inferred from GPS-derived surface velocities. J. Geophys. Res. Solid Earth. 118(2):709–23.

McCrory PA, Blair JL, Waldhauser F, Oppenheimer DH. 2012. Juan de Fuca slab geometry and its relation to Wadati-Benioff zone seismicity. J. Geophys. Res. Solid Earth. 117(B9).

McGuire JJ, Plank T, Barrientos S, Becker T, Brodsky E, Cottrell E. 2017. The SZ4D Initiative: Understanding the Processes that Underlie Subduction Zone Hazards in 4D. Vision Document Submitted to the National Science Foundation. The IRIS Consortium, 63 pp.

McNeill LC, Henstock TJ. 2014. Forearc structure and morphology along the Sumatra-Andaman subduction zone. Tectonics. 33(2):112–34.

Melgar D, Leveque RJ, Dreger DS, Allen RM. 2016. Kinematic rupture scenarios and synthetic displacement data: An example application to the Cascadia subduction zone. J. Geophys. Res. Solid Earth. 121:6658–74.

Meltzner AJ, Sieh K, Chiang H-W, Shen C-C, Suwargadi BW, et al. 2012. Persistent termini of 2004- and 2005-like ruptures of the Sunda megathrust. J. Geophys. Res. Solid Earth. 117(B4).

Meunier P, Hovius N, Haines AJ. 2007. Regional patterns of earthquake-triggered landslides and their relation to ground motion. Geophys. Res. Lett. 34(20):1–5.

Meunier P, Uchida T, Hovius N. 2013. Landslide patterns reveal the sources of large earthquakes. Earth Planet. Sci. Lett. 363:27–33.

Michel S, Gualandi A, Avouac JP. 2018. Interseismic coupling and slow slip events on the Cascadia megathrust. Pure and Applied Geophysics, 176, 3867–3891.

Milker Y, Nelson AR, Horton BP, Engelhart SE, Bradley LA, et al. 2016. Differences in coastal subsidence in southern Oregon (USA) during at least six prehistoric megathrust earthquakes. Quat. Sci. Rev. 142:143-163.

Moernaut J, van Daele M, Fontijn K, Heirman K, Kempf P, et al. 2018. Larger earthquakes recur more periodically: New insights in the megathrust earthquake cycle from lacustrine turbidite records in south-central Chile. Earth Planet. Sci. Lett. 481:9–19.

Morey AE, Goldfinger C, Briles CE, Gavin DG, Colombaroli D, Kusler JE. 2013. Are great Cascadia earthquakes recorded in the sedimentary records from small forearc lakes? Nat. Hazards Earth Syst. Sci. 13(10):2441–63.

Mountjoy JJ, Howarth JD, Orpin AR, Barnes PM, Bowden DA, et al. 2018. Earthquakes drive large-scale submarine canyon development and sediment supply to deep-ocean basins. Sci. Adv. 4(3): 3748.

Nelson AR, Atwater BF, Bobrowsky PT, Bradley L-A, Clague JJ, et al. 1995. Radiocarbon evidence for extensive plate-boundary rupture about 300 years ago at the Cascadia subduction zone. Nature. 378(6555):371–74.

Nelson AR, Shennan I, Long AJ. 1996. Identifying coseismic subsidence in tidal-wetland stratigraphic sequences at the Cascadia subduction zone of western North America. J. Geophys. Res. Solid Earth. 101(B3):6115–35.

Nelson AR, Kelsey HM, Witter RC. 2006. Great earthquakes of variable magnitude at the Cascadia subduction zone. Quat. Res. 65(3):354–65.

Nelson AR, Sawai Y, Jennings AE, Bradley LA, Gerson L, et al. 2008. Great-earthquake paleogeodesy and tsunamis of the past 2000 years at Alsea Bay, central Oregon coast, USA. Quat. Sci. Rev. 27(7–8):747–68.

Nelson AR, Hawkes AD, Sawai Y, Horton BP, Witter R, et al. In review. Minimal stratigraphic evidence for earthquake subsidence signals 2000 years of variable megathrust rupture modes at the central Cascadia subduction zone. Geosphere.

Nelson AR, Hawkes AD, Sawai Y, Engelhart SE, Witter R, et al. 2020. Identifying the greatest earthquakes of the past 2000 years at the Nehalem river Estuary, northern Oregon coast, USA. Open Quat. 6(2):1–30.

Newman AV, Okal EA. Teleseismic estimates of radiated seismic energy: The E/M0 discriminant for tsunami earthquakes. J. Geophys. Res. 103(B11):26885-26898.

Nocquet JM, Jarrin P, Vallée M, Mothes PA, Grandin R, et al. 2017. Supercycle at the Ecuadorian subduction zone revealed after the 2016 Pedernales earthquake. Nat. Geosci. 10(2):145–49.

Obara K, Kato A. 2016. Connecting slow earthquakes to huge earthquakes. Science. 353(6296):253-257.

Obermeier SF, Atwater BF, Benson BE, Peterson CD, Moses LJ, Pringle PT, Palmer SP. 1993. Liquefaction about 300 Years Ago Along Tidal Marshes of the Columbia River, Oregon and Washington. Transactions of American Geophysical Union EOS. 74:198.

Obermeier SF. 1995. Preliminary estimates of the strength of prehistoric shaking in the Columbia River Valley and the southern half of coastal Washington, with emphasis for a Cascadia subduction zone earthquake about 300 years ago. US Geological Survey Open-File Report. 94:589.

Obermeier SF, Dickenson SE. 2000. Liquefaction Evidence for the Strength of Ground Motions Resulting from Late Holocene Cascadia Subduction Earthquakes, with Emphasis on the Event of 1700 A.D. Bull. Seismol. Soc. Am. 90(4):876–96.

Padgett JS, Engelhart SE, Kelsey HM, Witter RC, Cahill N, et al. In review. Timing and amount of southern Cascadia earthquake subsidence over the past 1,700 years at northern Humboldt Bay, California, USA. Geol. Soc. Am. Bull.

Pearl JK, Keck JR, Tintor W, Siekacz L, Herrick HM, et al. 2020a. New frontiers in tree-ring research. The Holocene. 30(6): 923 - 941.

Pearl JK, Anchukaitis KJ, Donnelly JP, Pearson C, Pederson N, et al. 2020b. A late Holocene subfossil Atlantic white cedar tree-ring chronology from the northeastern United States. Quat. Sci. Rev. 228:106104.

Pearson C, Salzer M, Wacker L, Brewer P, Sookdeo A, Kuniholm P. 2020. Securing timelines in the ancient Mediterranean using multiproxy annual tree-ring data. Proc. Natl. Acad. Sci. 117(15):8410 – 8415.

Perkins JP, Roering JJ, Burns WJ, Strubel W, Black BA, et al. 2018. Hunting for landslides from Cascadia's great earthquakes. Eos. 99.

Peters R, Jaffe B, Gelfenbaum G. 2007. Distribution and sedimentary characteristics of tsunami deposits along the Cascadia margin of western North America: Sediment. Geol. 200:372–386, doi: 10.1016/j.sedgeo.2007.01.015.

Petersen MD, Cramer CH, Frankel AD. 2002. Simulations of seismic hazard for the Pacific Northwest of the United States from earthquakes associated with the Cascadia subduction zone. Pure Appl. Geophys. 159(9):2147–68.

Peterson CD, Carver GA, Cruikshank KM, Abramson HF, Garrison-Laney CE, et al. 2011. Evaluation of the use of paleotsunami deposits to reconstruct inundation distance and runup heights associated with prehistoric inundation events, Crescent City, southern Cascadia margin. Earth Surf. Proc. Land. 36(7):967-80.

Petersen MD, Moschetti MP, Powers PM, Mueller CS, Haller KM, et al. 2014. Documentation for the 2014 Update of the United States National Seismic Hazard Maps, US Geological Survey Open File Report 2014–1091.

Petersen MD, Shumway AM, Powers PM, Mueller CS, Moschetti MP, et al. 2019. The 2018 update of the US National Seismic Hazard Model: Overview of model and implications. Earthq. Spectra. 36(1):5–41.

Philibosian B, Meltzner AJ. 2020. Segmentation and supercycles: A catalog of earthquake rupture patterns from the Sumatran Sunda Megathrust and other well-studied faults worldwide. Quat. Sci. Rev. 241:106390.

Pollitz FF, Evans EL. 2017. Implications of the earthquake cycle for inferring fault locking on the Cascadia megathrust. Geophys. J. Int. 209(1):167–85.

Porritt RW, Allen RM, Boyarko DC, Brudzinski MR. 2011. Investigation of Cascadia segmentation with ambient noise tomography. Earth Planet. Sci. Lett. 309(1):67–76.

Praet N, Moernaut J, Van Daele M, Boes E, Haeussler PJ, et al. 2017. Paleoseismic potential of sublacustrine landslide records in a high-seismicity setting (south-central Alaska). Mar. Geol. 384:103–19.

Priest GR, Zhang Y, Witter RC, Wang K, Goldfinger C, Stimely L. 2014. Tsunami impact to Washington and northern Oregon from segment ruptures on the southern Cascadia subduction zone. Nat. Hazards. 72(2):849–70.

Reid HF. 1910. The mechanics of the earthquake, in The California Earthquake of April 18, 1906, Report of the State Earthquake Investigation Commission, 2:16-28.

Rogers G, Dragert H. 2003. Episodic Tremor and Slip on the Cascadia Subduction Zone: The Chatter of Silent Slip. Science. 300(5627):1942 LP – 1943.

Rong Y, Jackson DD, Magistrale H, Goldfinger C. 2014. Magnitude limits of subduction zone earthquakes. Bull. Seismol. Soc. Am. 104(5):2359-77.

Roten D, Olsen KB, Takedatsu R. 2019. Numerical Simulation of M9 Megathrust Earthquakes in the Cascadia Subduction Zone. Pure Appl. Geophys. 177(2020):2125–2141.

Saffer DM, Bekins BA. 2002. Hydrologic controls on the morphology and mechanics of accretionary wedges. Geology. 30(3):271–74.

Sahakian VJ, Melgar D, Muzli M. 2019. Weak near-field behavior of a tsunami earthquake: Toward real-time identification for local warning. Geophysical Research Letters. 46(16):9519-9528.

Saillard M, Audin L, Rousset B, Avouac JP, Chlieh M, et al. 2017. From the seismic cycle to long-term deformation: linking seismic coupling and Quaternary coastal geomorphology along the Andean megathrust. Tectonics. 36(2):241–56.

Satake K, Wang K, Atwater BF. 2003. Fault slip and seismic moment of the 1700 Cascadia earthquake inferred from Japanese tsunami descriptions. J. Geophys. Res. Solid Earth. 108(B11).

Schmalzle GM, McCaffrey R, Creager KC. 2014. Central Cascadia subduction zone creep. Geochemistry, Geophys. Geosystems. 15(4):1515–1.

Scholz CH. 2014. Holocene Earthquake History of Cascadia: A Quantitative Test. Bull. Seismol. Soc. Am. 104(4):2120–24.

Schulz WH, Galloway SL, Higgins JD. 2012. Evidence for earthquake triggering of large landslides in coastal Oregon, USA. Geomorphology. 141–142:88–98.

Schwartz DP, Coppersmith KJ. 1984. Fault behavior and characteristic earthquakes: Examples from the Wasatch and San Andreas Fault Zones. J. Geophys. Res. Solid Earth. 89(B7):5681–98.

Shimazaki K, Nakata T. 1980. Time-predictable recurrence model for large earthquakes. Geophys. Res. Lett. 7(4):279–82.

Shennan I, Long AJ, Rutherford MM, Green FM, Innes JB, et al. 1996. Tidal marsh stratigraphy, sea-level change and large earthquakes, I: A 5000 year record in Washington, U.S.A. Quat. Sci. Rev. 15(10):1023–59.

Shennan I, Scott DB, Rutherford M, Zong Y. 1999. Microfossil analysis of sediments representing the 1964 earthquake, exposed at Girdwood Flats, Alaska, USA. Quat. Int. 60(1):55–73.

Shennan I, Garrett E, Barlow N. 2016. Detection limits of tidal-wetland sequences to identify variable rupture modes of megathrust earthquakes. Quat. Sci. Rev. 150:1–30.

Sieh K, Natawidjaja DH, Meltzner AJ, Shen CC, Cheng H, et al. 2008. Earthquake supercycles inferred from sea-level changes recorded in the corals of west Sumatra. Science. 322(5908):1674–78.

Stone I, Vidale JE, Han S, Roland E. 2018. Catalog of Offshore Seismicity in Cascadia: Insights Into the Regional Distribution of Microseismicity and its Relation to Subduction Processes. J. Geophys. Res. Solid Earth. 123(1):641–52.

Struble WT, Roering JJ, Black BA, Burns WJ, Calhoun N, Wetherell L. 2020. Dendrochronological dating of landslides in western Oregon: Searching for signals of the Cascadia AD 1700 earthquake. Geol. Soc. Am. Bull. 132(7-8):1775–1791.

Sykes LR, Menke W. 2006. Repeat Times of Large Earthquakes: Implications for Earthquake Mechanics and Long-Term Prediction. Bull. Seismol. Soc. Am. 96(5):1569–96.

Takada K, Atwater BF. 2004. Evidence for liquefaction identified in peeled slices of Holocene deposits along the Lower Columbia River, Washington. Bull. Seismol. Soc. Am. 94(2):550–75.

Tréhu AM. 2016. Source Parameter Scaling and the Cascadia Paleoseismic Record. Bull. Seismol. Soc. Am. 106(3):904-11.

Tréhu AM, Asudeh I, Brocher TM, Luetgert JH, Mooney WD, et al. 1994. Crustal architecture of the Cascadia forearc. Science. 266(5183):237-43.

Tréhu AM, Blakely RJ, Williams MC. 2012. Subducted seamounts and recent earthquakes beneath the central cascadia forearc. Geology. 40(2):103–6.

Tréhu AM, Braunmiller J, Davis E. 2015. Seismicity of the Central Cascadia Continental Margin near 44.5° N: A Decadal View. Seismol. Res. Lett. 86(3):819–29.

Tréhu AM, Hass B, de Moor A, Maksymowicz A, Contreras-Reyes E, et al. 2019. Geologic controls on up-dip and along-strike propagation of slip during subduction zone earthquakes from a high-resolution seismic reflection survey across the northern limit of slip during the 2010 Mw 8.8 Maule earthquake, offshore Chile. Geosphere. 15(6):1751-73.

van Daele M, Araya-Cornejo C, Pille T, Vanneste K, Moernaut J, et al. 2019. Distinguishing intraplate from megathrust earthquakes using lacustrine turbidites. Geology. 47(2):127–30.

Vandekerkhove E, van Daele M, Praet N, Cnudde V, Haeussler PJ, et al. 2020. Flood-triggered versus earthquake-triggered turbidites: A sedimentological study in clastic lake sediments (Eklutna Lake, Alaska). Sedimentology. 67(1):364–89.

Veblen TT, Ashton DH. 1978. Catastrophic influences on the vegetation of the Valdivian Andes, Chile. Vegetation. 36(3):149–67.

Victor P, Sobiesiak M, Glodny J, Nielsen SN, Oncken O. 2011. Long-term persistence of subduction earthquake segment boundaries: Evidence from Mejillones Peninsula, northern Chile. J. Geophys. Res. Solid Earth. 116(B2).

von Huene R, Scholl DW. 1991. Observations at convergent margins concerning sediment subduction, subduction erosion, and the growth of continental crust. Rev. Geophys. 29(3):279–316.

Wang D, Mori J. 2011. Frequency-dependent energy radiation and fault coupling for the 2010 Mw8.8 Maule, Chile, and 2011 Mw9.0 Tohoku, Japan, earthquakes. Geophys. Res. Lett. 38(22):1–6.

Wang K, Tréhu AM. 2016. Invited review paper: Some outstanding issues in the study of great megathrust earthquakes—The Cascadia example. J. Geodyn. 98:1–18.

Wang K, Wells R, Mazzotti S, Hyndman RD, Sagiya T, 2003. A revised dislocation model of interseismic deformation of the Cascadia subduction zone. Journal of Geophysical Research: Solid Earth. 108(B1).

Wang PL, Engelhart SE, Wang K, Hawkes AD, Horton BP, et al. 2013. Heterogeneous rupture in the great Cascadia earthquake of 1700 inferred from coastal subsidence estimates. J. Geophys. Res. Solid Earth. 118(5):2460–73.

Wartman J, Dunham L, Tiwari B, Pradel D. 2013. Landslides in Eastern Honshu Induced by the 2011 Tohoku Earthquake. Bull. Seismol. Soc. Am. 103(2B):1503–21.

Watt JT, Brothers DS. 2020. Systematic characterization of morpho-tectonic variability along the Cascadia convergent margin: implications for shallow megathrust behavior and hazards. Geosphere.

Wells RE, Weaver CS, Blakely RJ. 1998. Fore-arc migration in Cascadia and its neotectonic significance. Geology. 26(8):759-62.

Wells RE, Blakely RJ, Sugiyama Y, Scholl DW, Dinterman PA. 2003. Basin-centered asperities in great subduction zone earthquakes: A link between slip, subsidence, and subduction erosion? J. Geophys. Res. Solid Earth. 108(B10).

Wells RE, Blakely RJ, Wech AG, McCrory PA, Michael A. 2017. Cascadia subduction tremor muted by crustal faults. Geology. 45(6):515–18.

Williams HF, Hutchinson I, Nelson AR. 2005. Multiple sources for late-Holocene tsunamis at Discovery Bay, Washington State, USA. The Holocene. 15(1):60-73.

Wirth EA, Frankel AD. 2019. Impact of down-dip rupture limit and high-stress drop subevents on coseismic land-level change during Cascadia Megathrust earthquakes. Bull. Seismol. Soc. Am. 109(6):2187–97.

Wirth EA, Frankel AD, Marafi N, Vidale JE, Stephenson WJ. 2018. Broadband Synthetic Seismograms for Magnitude 9 Earthquakes on the Cascadia Megathrust Based on 3D Simulations and Stochastic Synthetics, Part 2: Rupture Parameters and Variability. Bull. Seismol. Soc. Am. 108(5A):2370–88.

Witter RC, Kelsey HM, Hemphill-Haley E. 2003. Great Cascadia earthquakes and tsunamis of the past 6700 years, Coquille River estuary, southern coastal Oregon. Bull. Geol. Soc. Am. 115(10):1289–1306.

Witter RC, Zhang Y, Wang K, Goldfinger C, Priest GR, Allan JC. 2012a. Coseismic slip on the southern Cascadia megathrust implied by tsunami deposits in an Oregon lake and earthquake-triggered marine turbidites. J. Geophys. Res. Solid Earth. 117(B10).

Witter RC, Jaffe B, Zhang Y, Priest G, 2012b. Reconstructing hydrodynamic flow parameters of the 1700 tsunami at Cannon Beach, Oregon, USA. Natural Hazards. 63(1):223-40.

Witter RC, Zhang YJ, Wang K, Priest GR, Goldfinger C, et al., 2013. Simulated tsunami inundation for a range of Cascadia megathrust earthquake scenarios at Bandon, Oregon, USA. Geosphere. 1;9(6):1783-803.

Wong FL, Grim MS, 2015. Depth-to-Basement, Sediment-Thickness, and Bathymetry Data for the Deep-Sea Basins Offshore of Washington, Oregon, and California. United States Geological Survey Open File Report 2015-1118.

Yamaguchi DK, Atwater BF, Bunker DE, Benson BE, Reid MS. 1997. Tree-ring dating the 1700 Cascadia earthquake. Nature. 389(6654):922–23.

Ye L, Lay T, Kanamori H, Rivera L. 2016. Rupture characteristics of major and great (Mw≥ 7.0) megathrust earthquakes from 1990 to 2015: 2. Depth dependence. J. Geophys. Res. 121(2):845-63.

Yousefi M, Milne G, Li S, Wang K, Bartholet A. 2020. Constraining Interseismic Deformation of the Cascadia Subduction Zone: New Insights From Estimates of Vertical Land Motion Over Different Timescales. J. Geophys. Res. Solid Earth. 125(3):e2019JB018248.

Zielke O. 2018. Earthquake Recurrence and the Resolution Potential of Tectono-Geomorphic Records. Bull. Seismol. Soc. Am. 108(3A):1399–1413.

Terms and definitions

Recurrence interval: The average time span between significant earthquake occurrences on a fault or in an earthquake source zone.

Evidence threshold: Criteria that must be exceeded in order to create and preserve a geologic signature of an event (earthquake).

Turbidites: Disturbance layers and evidence for turbidity currents (density flows) in marine or lacustrine environments.

Mud turbidites: Turbidite deposits that lack a sandy component.

Confluence test: A physiographic criterion used to correlate turbidites across a margin by comparing deposits in tributary and master channels.

Seismogenic zone: The part of the plate boundary located from ~15-35 km depths that tends to rupture in large earthquakes.

Stick-slip behavior: The frictional behavior required to generate an earthquake; where dynamic friction is less than the static friction.

Coupled zone: A geodetically inferred proxy for the seismogenic zone.

Rupture patch: The area on the megathrust that slips during a particular earthquake.

Rupture boundaries: Heterogeneities in physical properties that may inhibit earthquake rupture propagation over multiple earthquake cycles.

Tsunami earthquakes: Earthquakes in which shallow (depths less than ~15 km) slip occurs offshore, generating tsunamis.

Episodic tremor and slip: The phenomenon of seismically measured tremor that accompanies geodetically observed slip along a plate interface.

Supercycles: Nested clusters of subduction zone earthquakes.

Significant events: Fault slip events that relieve enough stress to permit statistical renewal of the recurrence process.

Serial ruptures: A series of adjacent earthquakes along a margin separated by short time intervals (days to decades).

Aleatoric variability: The irreducible intrinsic natural variability of a system.

Epistemic uncertainty: Reducible uncertainties that stem from limited knowledge.

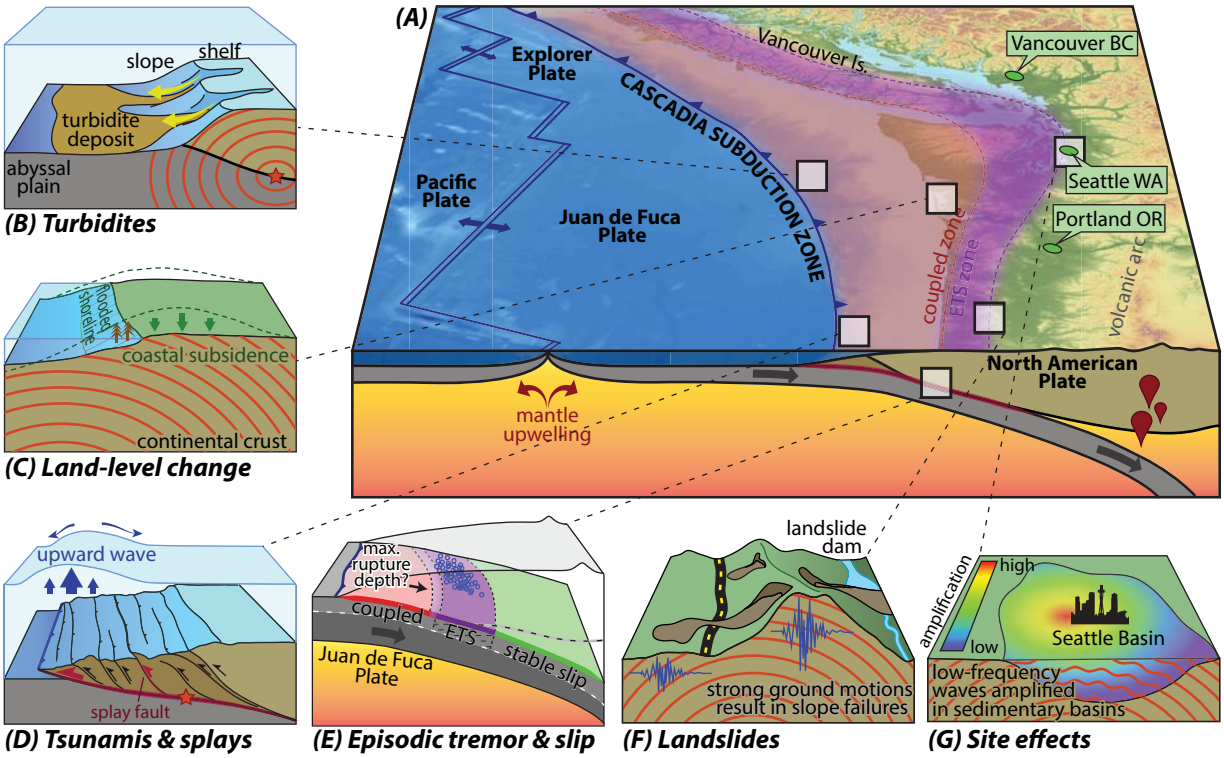

Figure 1. (A) Oblique view of the northwest margin of North American, where the Juan de Fuca and Explorer oceanic plates subduct beneath the North American Plate. On the side view, the thin red line between the two tectonic plates represents the region where great earthquakes occur. On the map overlay, the toothed blue line represents the surface trace of the where the subducting plate begins its descent. Major cities are shown as green dots. The purple swath shows the general region where episodic tremor and slip (ETS) occurs and the pink swath shows the general region considered to be the coupled zone. To the left and below (A), small diagrams illustrate various earthquake-related processes labeled beneath each diagram: (B) coseismic turbidite generation, (C) coseismic subsidence with dotted green line showing the pre-event coastal land-level, dead brown trees represent marine incursion onto a formerly terrestrial environment (D) and tsunami generation, (E) the relationship between the coupled fault and the ETS zone, with an ETS swarm depicted as blue circles, with a possible gap between the coupled zone and updip extent of ETS shown as a gradational area (F) coseismic landslide hazards, with schematic seismograms (in blue) showing the potential for topographic effects on ground motion amplification, and (G) how geologic features, such as sedimentary basins, can amplify seismic waves.

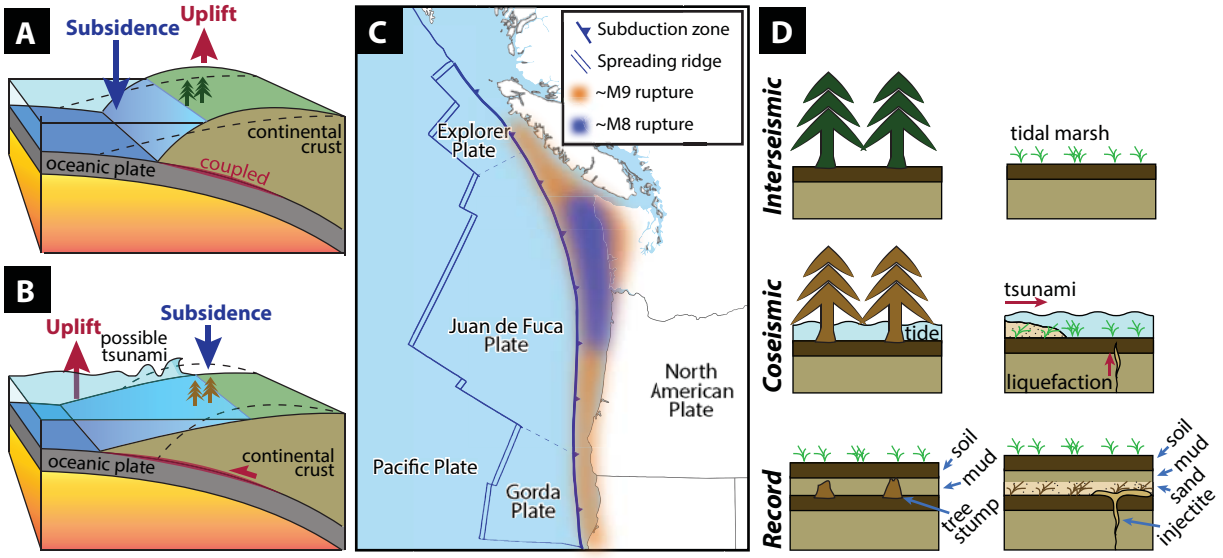

Figure 2. (A) Block diagram of the interseismic period, when convergence along the coupled subduction zone interface (red zone) typically causes gradual uplift in the onshore overriding plate, and gradual subsidence offshore. (B) Diagram of the coseismic period, when earthquake rupture along the subduction zone interface relieves accumulated strain and generally causes sudden subsidence in the onshore overriding place and sudden uplift in the offshore overriding plate. Shallow rupture may generate a tsunami. (C) Possible scenarios for an ~M9 (orange) and ~M8 (blue) events that rupture the CSZ plate interface. (D) Schematic diagrams of stratigraphic evidence for the earthquake deformation cycle. Left column shows the effect of coseismic subsidence on wetland stratigraphy and coastal forests and their preservation in the stratigraphic record (see also Fig. 1C). Right column shows stratigraphic preservation of coseismic tsunami deposits and liquefaction injectites.

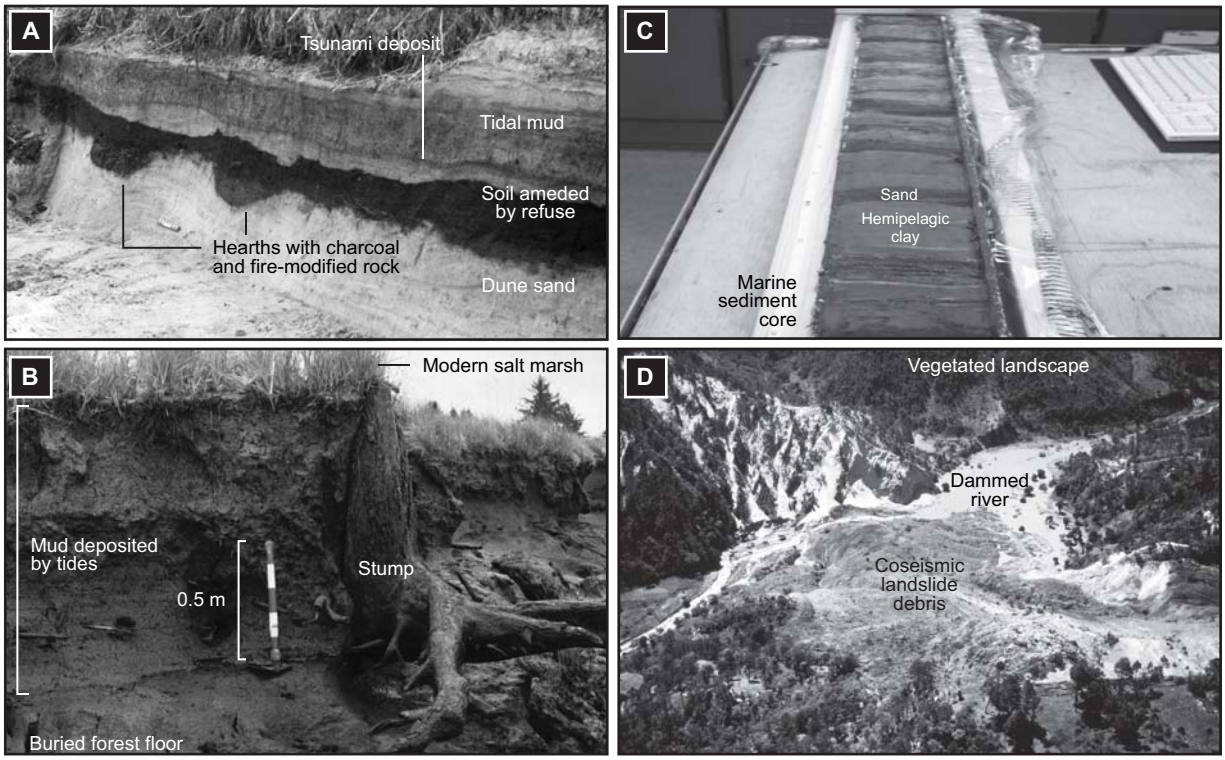

Figure 3. (A) Evidence for coseismic subsidence and tsunami inundation from a sedimentary exposure of subaerial dune sand and prehistoric settlements overlain by tsunami sand and tidal mud along the Salmon River, Oregon (Atwater et al., 2005). (B) Coseismic subsidence evidence from a drowned tree stump surrounded by tidal mud in the Naselle River near Willapa Bay (Atwater et al., 2005). (C) Marine sediment core showing dark bands of sandy sediment, interpreted as coseismic turbidite deposits, interbedded with lighter colored hemipelagic clay. Photo by C. Goldfinger. (D) An example of a coseismic landslide that dammed a river to produce a "quake lake", from the 1976 Guatemala earthquake (Espinosa, 1976). While not an example of coseismic landsliding in Cascadia, this photo demonstrates secondary hazard potential to the Pacific Northwest.

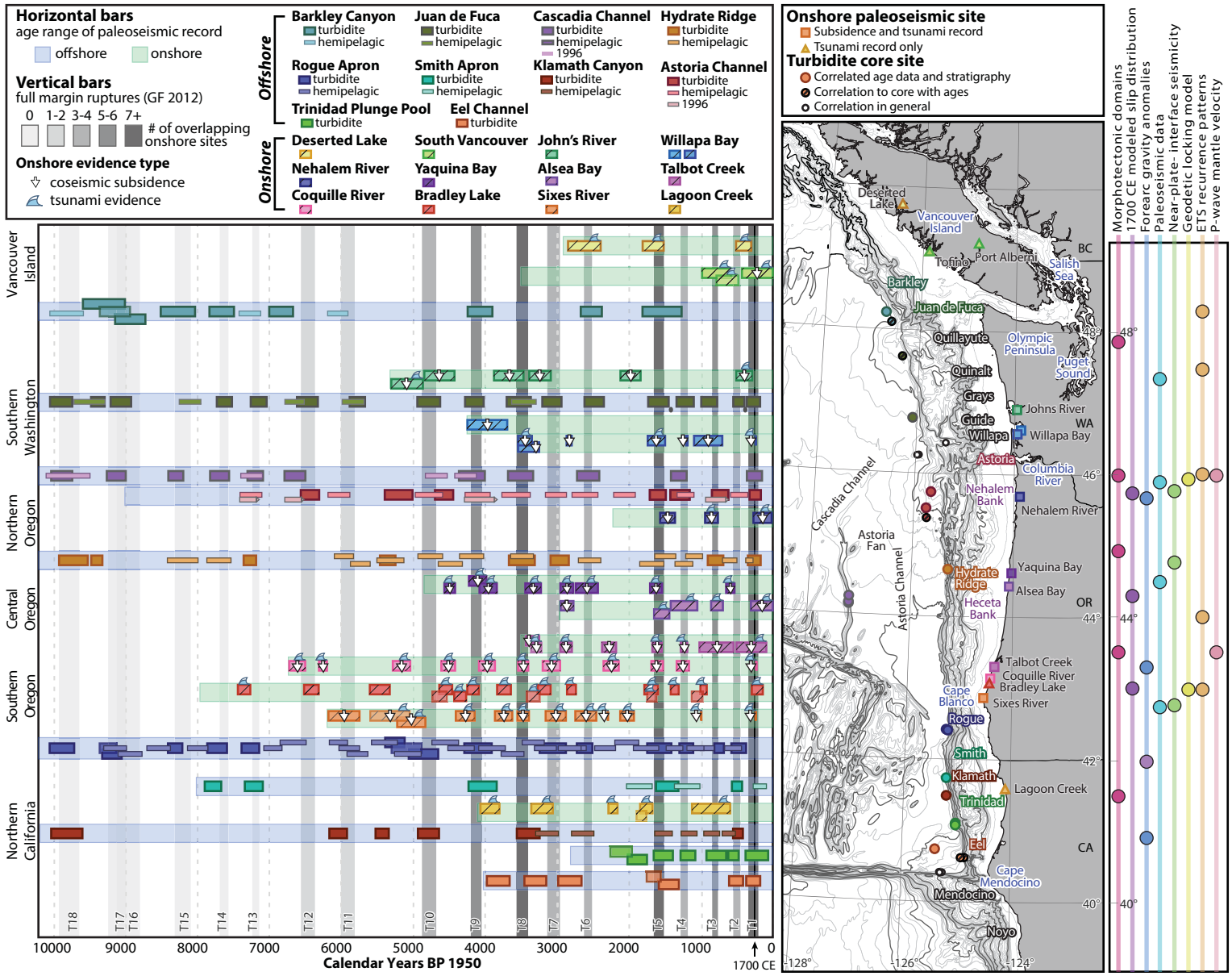
Horizontal bars
age range of paleoseismic record
offshore
onshore
Vertical bars
full margin ruptures (GF 2012)
0 1-2 3-4 5-6 7+
# of overlapping onshore sites
Onshore evidence type
coseismic subsidence
tsunami evidence
Offshore
Barkley Canyon
turbidite
hemipelagic
Juan de Fuca
turbidite
hemipelagic
Cascadia Channel
turbidite
hemipelagic
1996
Hydrate Ridge
turbidite
hemipelagic
Rogue Apron
turbidite
hemipelagic
Smith Apron
turbidite
hemipelagic
Klamath Canyon
turbidite
hemipelagic
Astoria Channel
turbidite
hemipelagic
1996
Trinidad Plunge Pool
turbidite
Eel Channel
turbidite
Onshore
Deserted Lake
South Vancouver
John's River
Willapa Bay
Nehalem River
Yaquina Bay
Alsea Bay
Talbot Creek
Coquille River
Bradley Lake
Sixes River
Lagoon Creek
Vancouver Island
Southern Washington
Northern Oregon
Central Oregon
Southern Oregon
Northern California
T18
T17
T16
T15
T14
T13
T12
T11
T10
T9
T8
T7
T6
T5
T4
T3
T2
T1
10000
9000
8000
7000
6000
5000
4000
3000
2000
1000
0
1700 CE
Calendar Years BP 1950
Onshore paleoseismic site
Subsidence and tsunami record
Tsunami record only
Turbidite core site
Correlated age data and stratigraphy
Correlation to core with ages
Correlation in general
Deserted Lake
Vancouver Island
Tofino
Port Alberni
Salish Sea
BC
Barkley
Juan de Fuca
Quillayute
Olympic Peninsula
Puget Sound
Quinalt
Grays
Johns River
Willapa
Willapa Bay
WA
Astoria
Columbia River
Cascadia Channel
Nehalem Bank
Nehalem River
Astoria Fan
Astoria Channel
Hydrate Ridge
Yaquina Bay
Alsea Bay
Heceta Bank
OR
Talbot Creek
Coquille River
Bradley Lake
Cape Blanco
Sixes River
Rogue
Smith
Klamath
Lagoon Creek
Trinidad
Eel
CA
Cape Mendocino
Mendocino
Noyo
48°
46°
44°
42°
40°
128°
126°
124°
Morphotectonic domains
1700 CE modeled slip distribution
Forearc gravity anomalies
Paleoseismic data
Near-plate- interface seismicity
Geodetic locking model
ETS recurrence patterns
P-wave mantle velocity

Figure 4. (Left) Onshore and offshore geologic evidence for CSZ megathrust rupture. Semi-transparent green and blue horizontal bars indicate the temporal length of each record. Onshore and offshore event age range estimates are color-coded with site location (map figure to the right). Offshore age ranges are from turbidites analyzed by Goldfinger et al., 2012. Thick horizontal age ranges are sandy marine turbidite ages estimated from 14C dating of hemipelagic sediments, estimated basal erosion, and inferred sedimentation rate for each geographic locale. Thin horizontal age ranges are calculated ages of interbedded hemipelagic sediment. All age ranges are 2σ uncertainty propagated through 14C age calibration and correction. Vertical grey bars are interpreted event ages from a land-marine age compilation, which takes several onshore geology sites into account with some, but not all, of the geochronologic and stratigraphic information from marine sediment cores (Goldfinger et al., 2012; Table S1). The shade of grey reflects the number of onshore sites plotted here that are consistent with this interpretation (darker = more overlapping onshore data). Age ranges for onshore geologic evidence shown with hatched fill. Age ranges for subsidence (white arrow) and/or tsunami deposit (cute little wave) events are calibrated 14C dates or from OxCal modeling. GF2012 refers to Goldfinger et al. (2012). (Middle) Map shows the locations of onshore and offshore study sites, colored location markers correlate with the age-range panel to the left. Offshore canyons labeled using white text with colored outlines that correlate with turbidite age range bars determined for turbidites associated with that canyon. Black text outlines denote canyon data lacking or not used. Core ID numbers are available in Figure S1. Marine cores shown are only those used for age dating or stratigraphic correlation; additional marine core locations are in Goldfinger et al., 2012. Nearshore geographic features labeled in purple. Onshore geographic features labeled in blue. Bathymetric contours are 100 meter spacing in light grey, 500 meter interval in dark grey (derived from Wong & Grim, 2015). (Right) North-south evidence for possible rupture boundaries inferred from geophysical datasets, adapted from Watt & Brothers (2020). Circles denote locations of observations of along-strike heterogeneities. Latitudes correspond to the map.

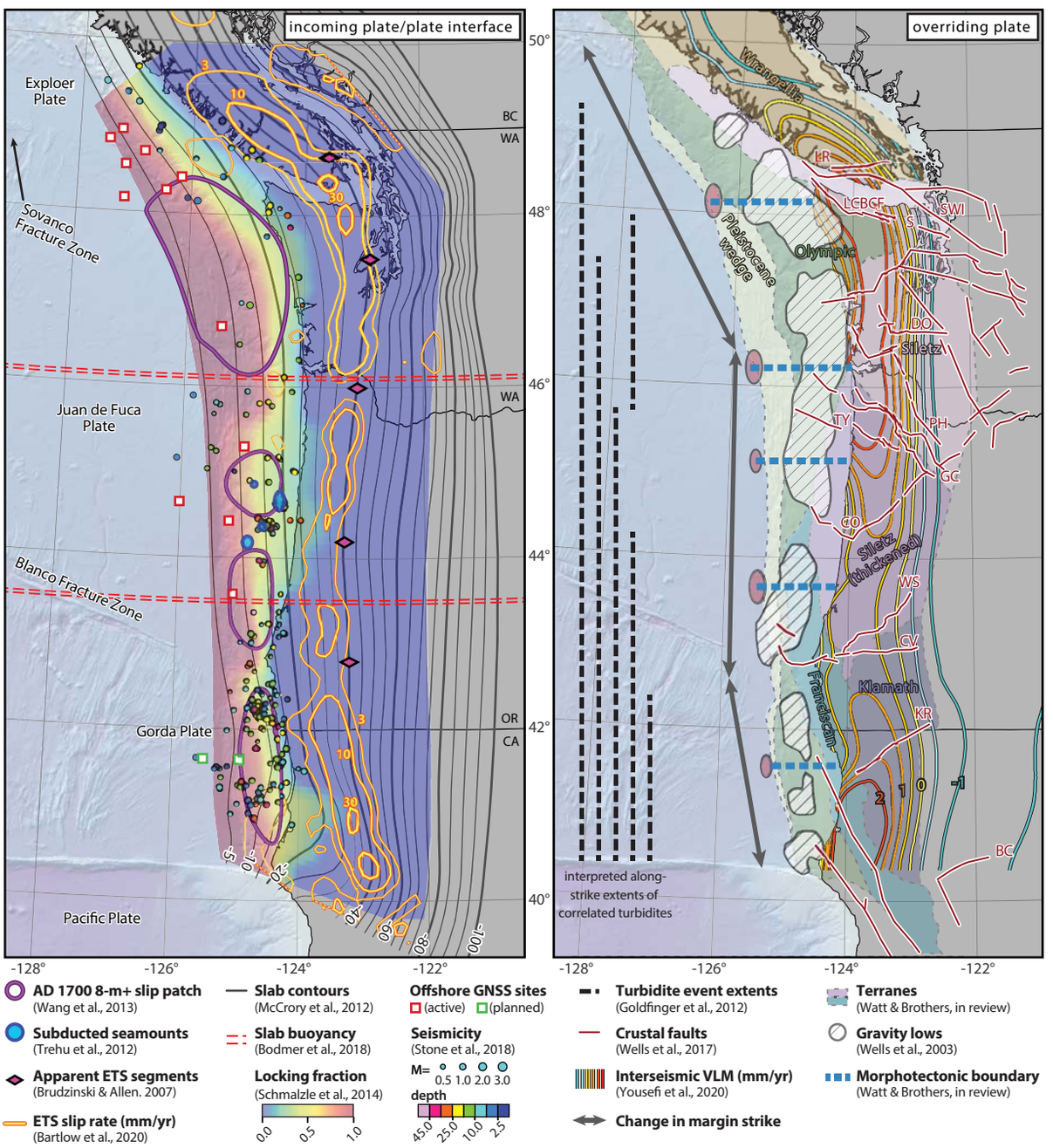

Figure 5. Maps of geophysical and geologic datasets used to infer along-strike heterogeneities along the CSZ. Left map shows heterogeneities on the incoming plate and plate interface. Time-averaged ETS slip rates from Bartlow (2020) are shown as contours with values from 30, 10, and 1 mm/yr. Seismicity from Stone et al. (2018) shows events associated with the CSZ, though note that earthquake depths are poorly constrained and some events may be located within the upper plate. Dense clusters of seismicity near latitudes 44.3° and 44.6° are coincident with subducted seamounts interpreted from magnetic and gravity anomalies (Trèhu et al., 2012). Right map shows heterogeneities on the overriding plate. Morphotectonic zones inferred do not necessarily have sharp boundaries (Watt & Brothers, 2020). VLM: Vertical Land Motion. Fault and lineament names: LR–Leech River fault; S–Seattlefault; SWI–South Whidbey Island fault; LCBC–Lake Creek Boundary Creek fault; DO–Doty fault; CR–Columbia River fault; GC–Gales Creek fault; TY–Tillamook-Yamhill fault; CO–Corvallis fault; WS–Wildlife Safari fault; CV–Canyonville fault; KR–Klamath River lineament; PH–Portland Hills fault; BC–Battle Creek fault. Bathymetric baselayer from Wong & Grim, 2015).

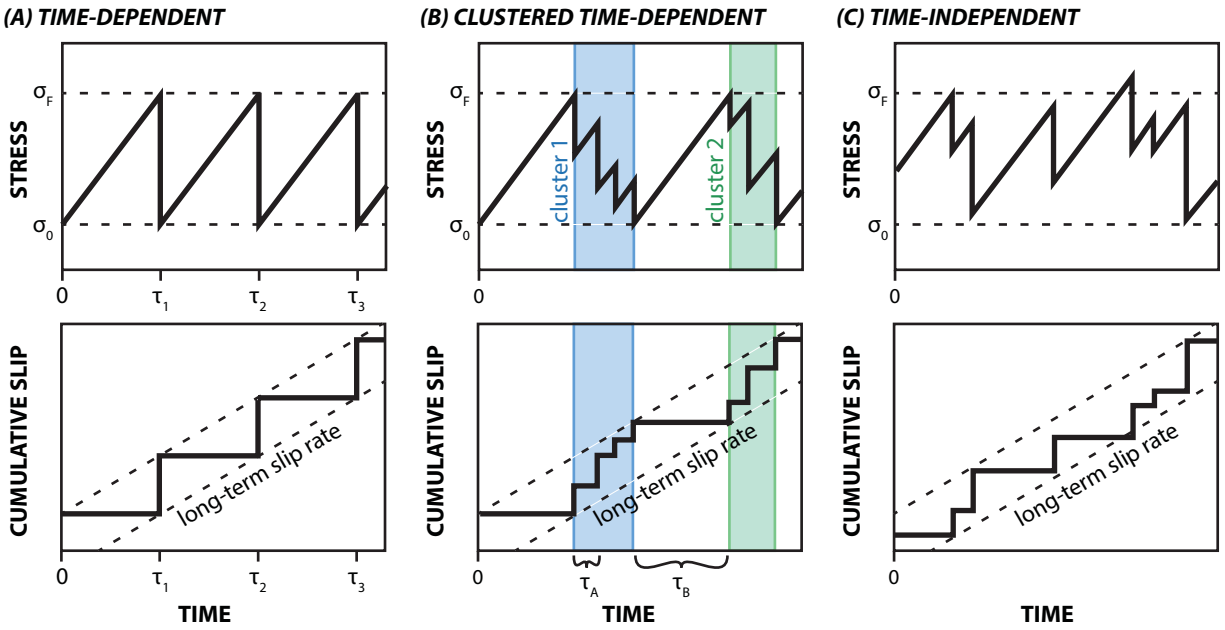

Figure 6. Schematic depiction of recurrence models often proposed for subduction zone settings. (A) Time-dependent model suggests periodic earthquake occurrence is dependent on steady long-term strain accumulation and failure at a critical stress level (i.e., from σO to σF). This model suggests predictable slip magnitude. (B) Clustered time-dependent model suggests earthquake recurrence is variable, with clustered occurrence earthquakes punctuated by longer intervals, τB, of seismic quiescence. Within a cluster, the probability of recurrence at return-interval of τA is high. Following a cluster, probability of recurrence decreases until the onset of the next cluster at return interval of τB. This model suggests long-term strain accumulation and slip rate may be similar to the periodic model, but that slip and timing is less predictable. (C) Time-independent models suggest that earthquake occurrence is unpredictable and may indicate that the displacement rate at the fault trace averaged over several consecutive earthquakes is non-linear.

Table 1. Characteristics of different earthquake recurrence models

	Time-independent	Time-dependent	
	Poisson	**Quasi-periodic**	**Clustered**
Event rate and periodicity	There is a general rate of occurence (e.g., 2 events per millenia), but events are not periodic	There is a rate of occurence and events are periodic	There is a rate of occurence and cycles are periodic. However, an earthquake cycle includes multiple superimposed cycles
Energy balance and stress release	Events independent of accumulated/released stress	Single-event cycle with characteristic magnitude releases sufficient accumulated stress to renew the statistical process	Stress accumulation and release balances over and earthquake cluster, or "supercycle"
Interevent time and probability	Random and unpredictable. Interevent time does not depend on slip rates or accummulated stress. There is equal probability for a 2 year and 200 year interevent time.	Consistent and predictable. Interevent time depends on strain accumulation rates. Probability of occurence increases as mean interevent time is approached	Interevent time depends on whether cluster is complete or in progress. Probability of occurence increases as either the mean 'intracluster' or 'extracluster' event times are approached
Hazard rate	Constant, independent of last event (memoryless)	Normal distribution around the expected event recurrence	Complex distribution around more than one event recurrence
COV	~1	<1	>1